The Center for BRIGHTBEAMS
A National Science Foundation Science & Technology Center

Photocathodes for ultra high-gradient NCRF guns

Gerard Lawler et al.

UCLA

U.S. DEPARTMENT OF ENERGY

Outline of presentation

1. Background and motivation
2. Electron emission considerations
3. Experimental results
4. Temperature dependence
5. Future directions
6. Conclusions

UCXFEL

- Our most pertinent realization of high gradient and high brightness techniques is Ultra-Compact Xray FEL (UCXFEL) concept (right)
- When combined with novel bunching and short period undulators we can approach 40m scales with several applications incl. allowing university scale XFEL access and chip metrology
- Existing plan incorporates cryogenically enabled >200 MV/m photoinjector peak fields and ≈ 70 MV/m linacs

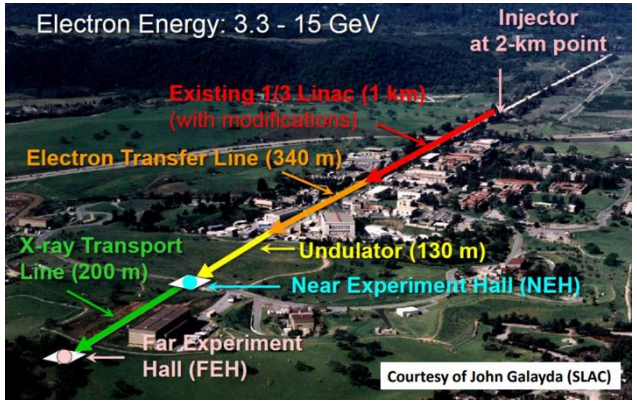

J. Galayda et al., "The new lcls-ii project: Status and challenges," in LINAC, 2014, pp. 404–408. [Online]. Available: https://accelconf.web.cern.ch/linac2014/talks/tuioa04_talk.pdf.

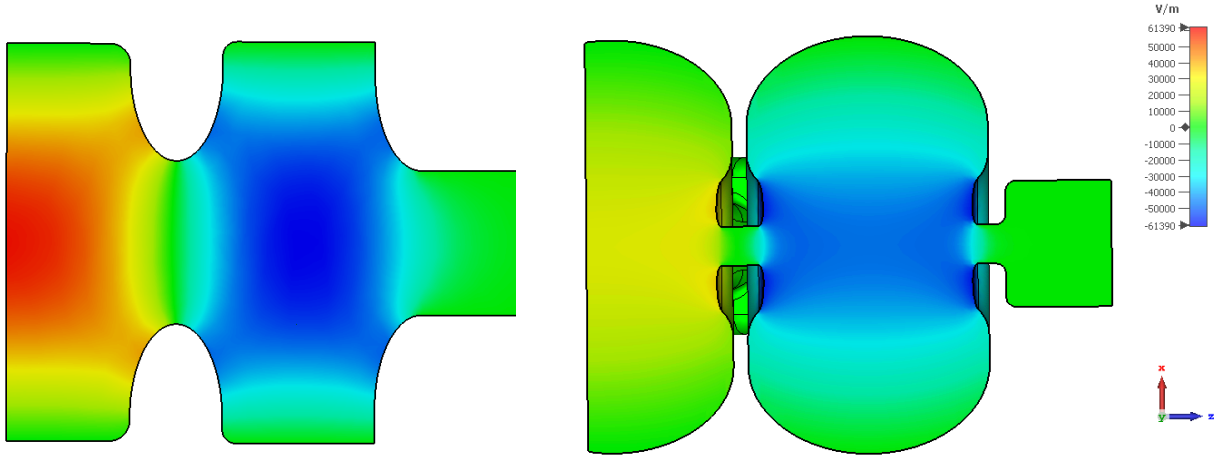

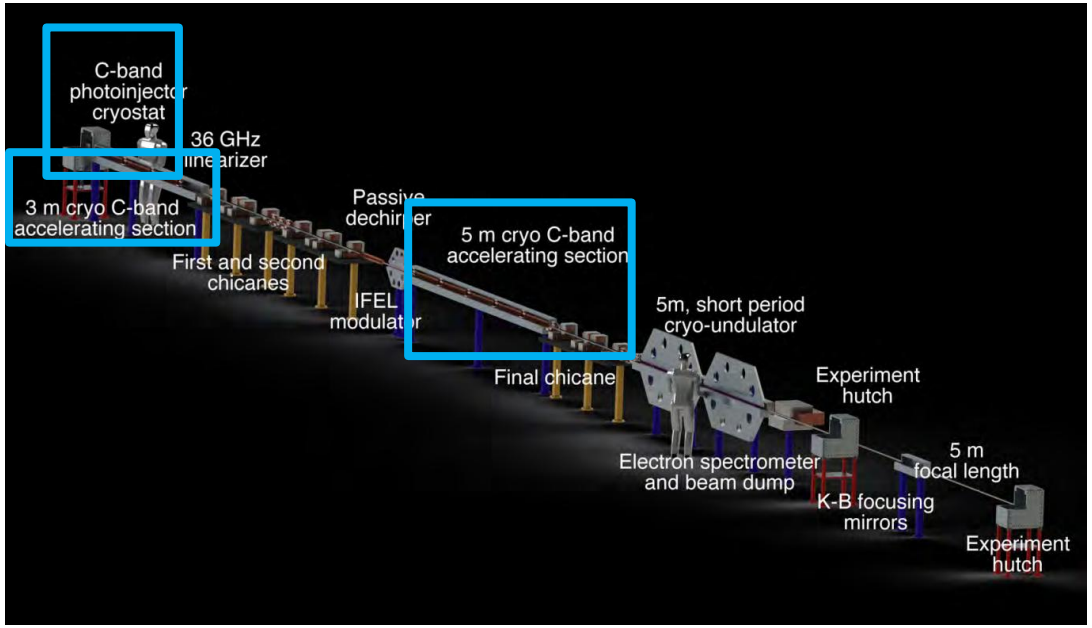

Rosenzweig, J. B. et al., *New Journal of Physics*, vol. 22, no. 9, p. 093067, 2020. doi:10.1088/1367-2630/abb16c

Cryogenic photogun brightness

- Limit to high gradient often breakdown rate (BDR)
- SLAC cryogenic breakdown reduction ⇒ higher accelerating gradients possible
- 1D space charge limited brightness scaling
  - Note launch field and temperature dependence
- *TopGun* previous development in S-band

Rosenzweig, J. B., et al. *Physical Review Accelerators and Beams* 22.2 (2019): 023403. Doi: 10.1103/PhysRevAccelBeams.22.023403%7

$$B_{e,b} \approx \frac{2ec\varepsilon_0}{k_B T_c}\left(E_0 \sin\varphi_0\right)^2$$

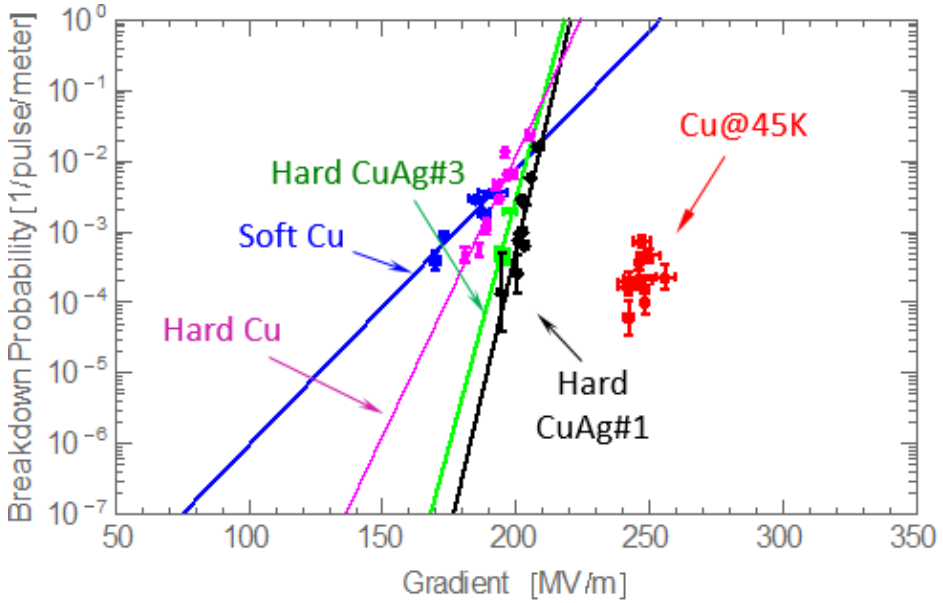

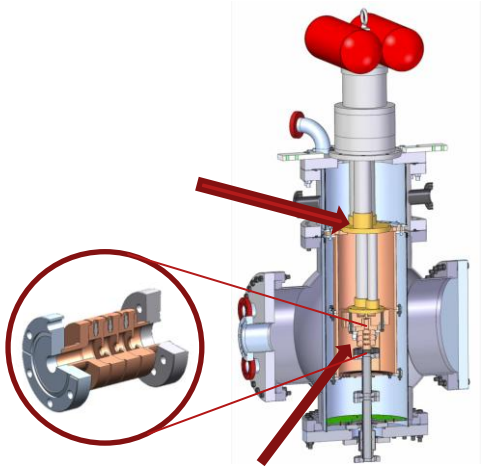

Cavities for high power test

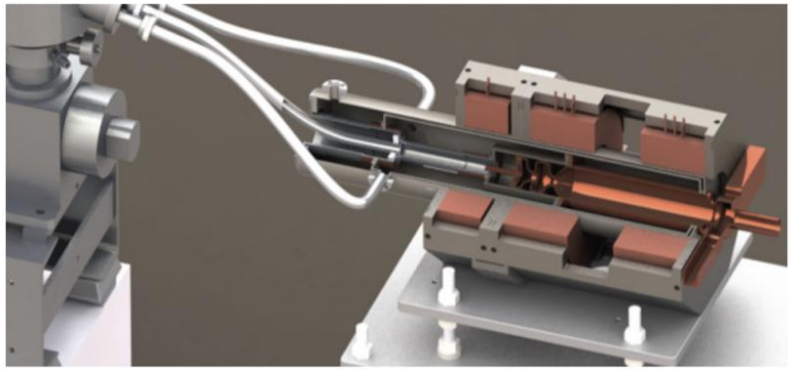

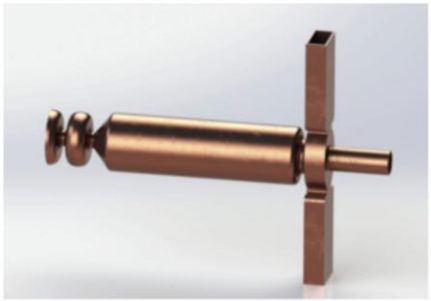

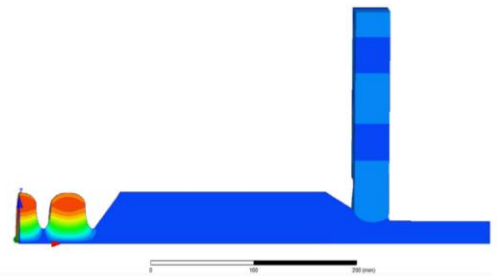

Cryo RF Performance Overview

- Parameters for gun thus far compared to RRR100-500 case (left) with empirical numbers measured to inform simulations (right)

Parameter	295K	100K	77K	40K
Frequency	5.695 GHz	5.711 GHz	5.712 GHz	5.713 GHz
Q_0	8579	18668	24200	39812
β	0.7	1.53	1.98	3.26
Filling time	-	0.41 μs	0.45 μs	0.52 μs

Lawler, G. E., et al. *Instruments* 8.1 (2024): 14.
Doi: 10.3390/instruments8010014

E field magnitude

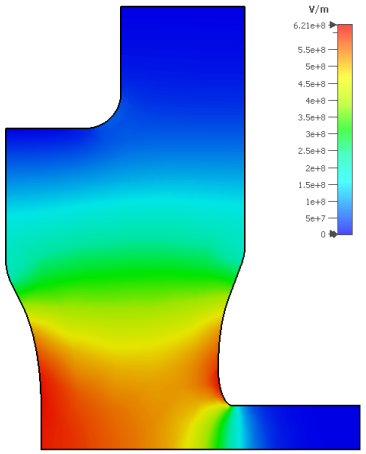

H field magnitude

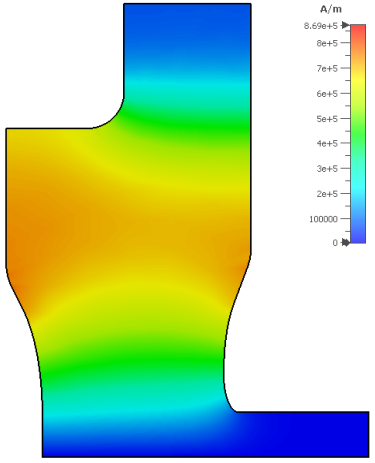

Parameter	295 K	95 K	77K	45 K
f_0 [MHz]	5703.6 ± 0.1[1]	5720.410 ± 0.003[1]	5721 ± 3	5722 ± 4
Q_0	7808 ± 13[1]	14326 ± 12[1]	21000 ± 3600	30000 ± 9900
Coupling β	0.608 ± 0.002[1]	1.069 ± 0.002[1]	1.60 ± 0.44	2.4 ± 0.9
Filling time [μs]	0.271 ± 0.01[1]	0.386 ± 0.001[1]	0.44 ± 0.01	0.49 ± 0.03
Power [MW] for 120 MV/m	1.23 ± 0.10	0.85 ± 0.08	0.79 ± 0.01	0.70 ± 0.09
Energy [J] per 2μs pulse	2.45 ± 0.01	1.70 ± 0.02	1.58 ± 0.03	1.40 ± 0.19
Cathode field @ 0.5 MW	77 ± 3 MV/m	92 ± 5 MV/m	93 ± 3 MV/m	102 ± 7 MV/m

[1] Values experimentally measured or computed directly from low power measurements

Gun Comparisons

- CYBORG design inspired primarily by 3 existing photoguns: PEGASUS; Cornell Cryo DC gun; FERMI
- Compared CYBORG design specs also with existing cathode test beds

Parameter	CYBORG Phase 1	CYBORG Phase 2
Cavity type	normal conducting	-
Cavity geometry	$\frac{1}{2}$-cell reentrant	-
Cathode Assembly	Demountable Cu backplate	Cryogenic load lock
Design frequency	5.712 GHz	5.700 – 5.720 GHz
Peak cathode field	$\geq$ 120 MV/m	-
Operating temperature	300 – 95K[1]	300 – 77K

[1] Current lowest temperature achieved with additional plans for 77 K operation

Photoguns	FERMI [20]	PEGASUS [6,21]	PITZ [22,23]	HZDR [24]/HZB [25]	Cornell [26]/ASU [27]	BNL [25,28]
Cavity type *	NCRF	NCRF	NCRF	SRF	-	SRF
Cavity geometry *	1.6 cell pillbox	1.6 cell pillbox	1.5 cell pillbox	1.5 cell elliptical	-	quarter wave
Cathode assembly	Demountable Cu backplate	Demountable Cu backplate + load-lock	Demountable Cu backplate + load-lock	Load-lock	Load-lock	Load-lock
Design frequency	2.998 GHz	2.856 GHz	1.3 GHz	1.3 GHz	DC	0.113 GHz
Peak cathode field	125 MV/m	120 MV/m (Cu backplate)	60 MV/m	15 – 20 MV/m	10 MV/m	10 – 15 MV/m
Min cathode T	$\geq$ room T	$\geq$ room T	$\geq$ room T	80 K	35 K	2 K

* Only relevant for RF guns.

Lawler, G. E., et al. *Instruments* 8.1 (2024): 14.
Doi: 10.3390/instruments8010014

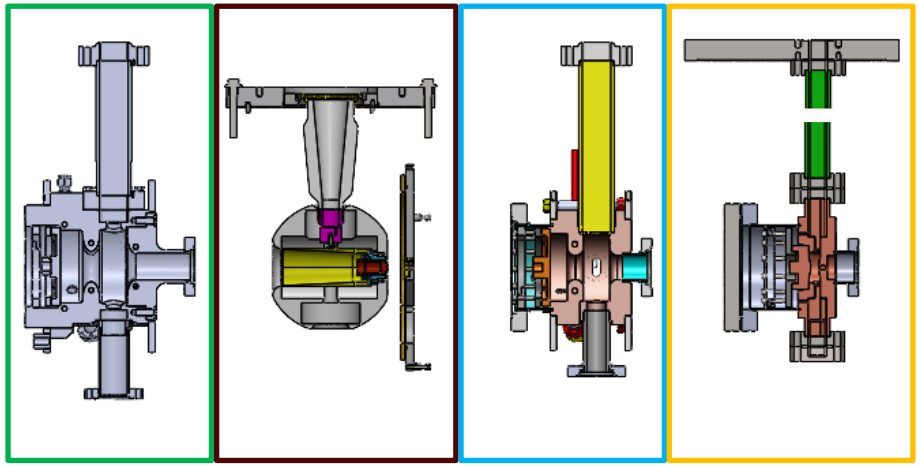

Dark current simulations

- Fowler-Nordheim field emission in particle-in-cell (PIC) simulation via CST with peak cathode plane gradient 60 MV/m and β = 50 needed for significant emission
- Further uniformity assumption

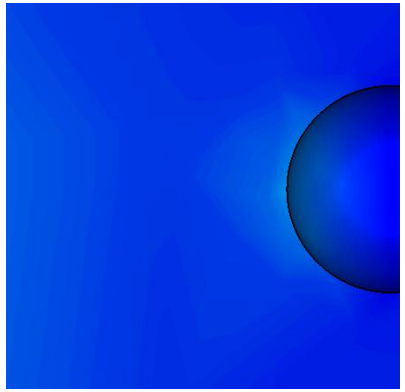

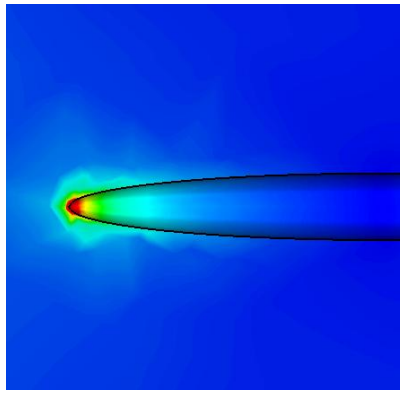

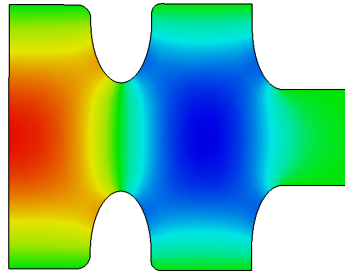

[arb. units]

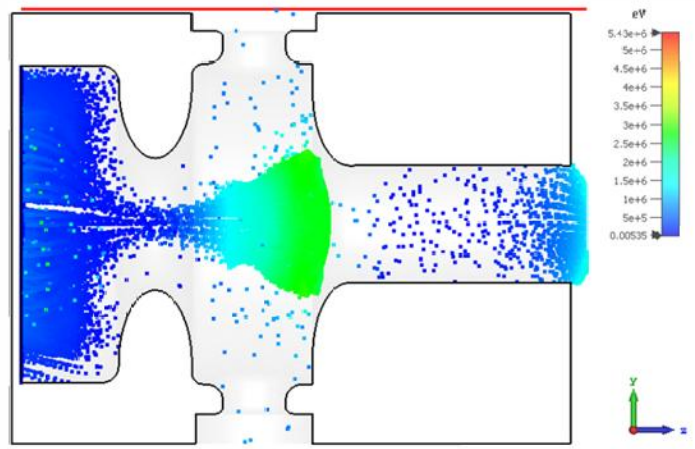

$$J_F(F) = \frac{A_0}{\Phi t_0^2}\left(\frac{\Phi^2 e^6}{4Q}\right)^v F^{2-v} \exp\left(\frac{-B_0\Phi^{3/2}}{F}\right)$$

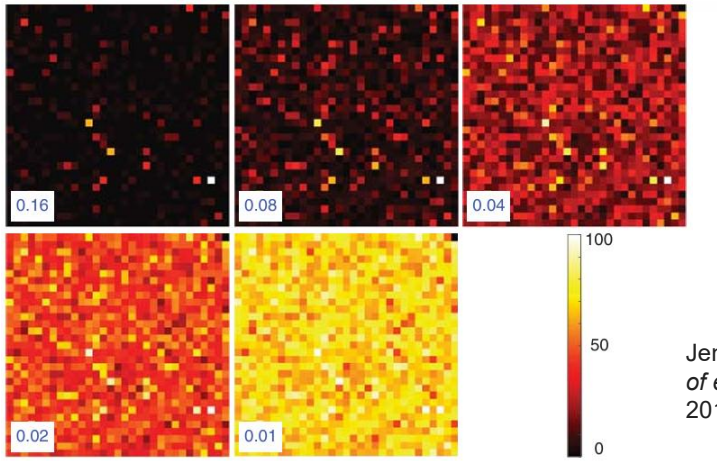

Lawler, GE. *Improvements to Normal Conducting High Gradient Accelerator Performance at Cryogenic Temperatures*. University of California, Los Angeles, 2024.

R. N. Allan and A. J. Salim, "Prebreakdown currents and breakdown voltages in vacuum at cryogenic temperatures," Journal of Physics D: Applied Physics, vol. 7, no. 8, p. 1159, May 1974. doi: 10.1088/0022-3727/7/8/313

Jensen, Kevin L. *Introduction to the physics of electron emission*. John Wiley & Sons, 2017.

Dark current simulation

- Fowler-Nordheim field emission in particle-in-cell (PIC) simulation via CST with peak cathode plane gradient 60 MV/m and β = 50 needed for significant emission
- Further uniformity assumption
- Increased capture in ½ cell reentrant geometry

$$J_F(F) = \frac{A_0}{\Phi t_0^2}\left(\frac{\Phi^2 e^6}{4Q}\right)^v F^{2-v} \exp\left(\frac{-B_0\Phi^{3/2}}{F}\right)$$

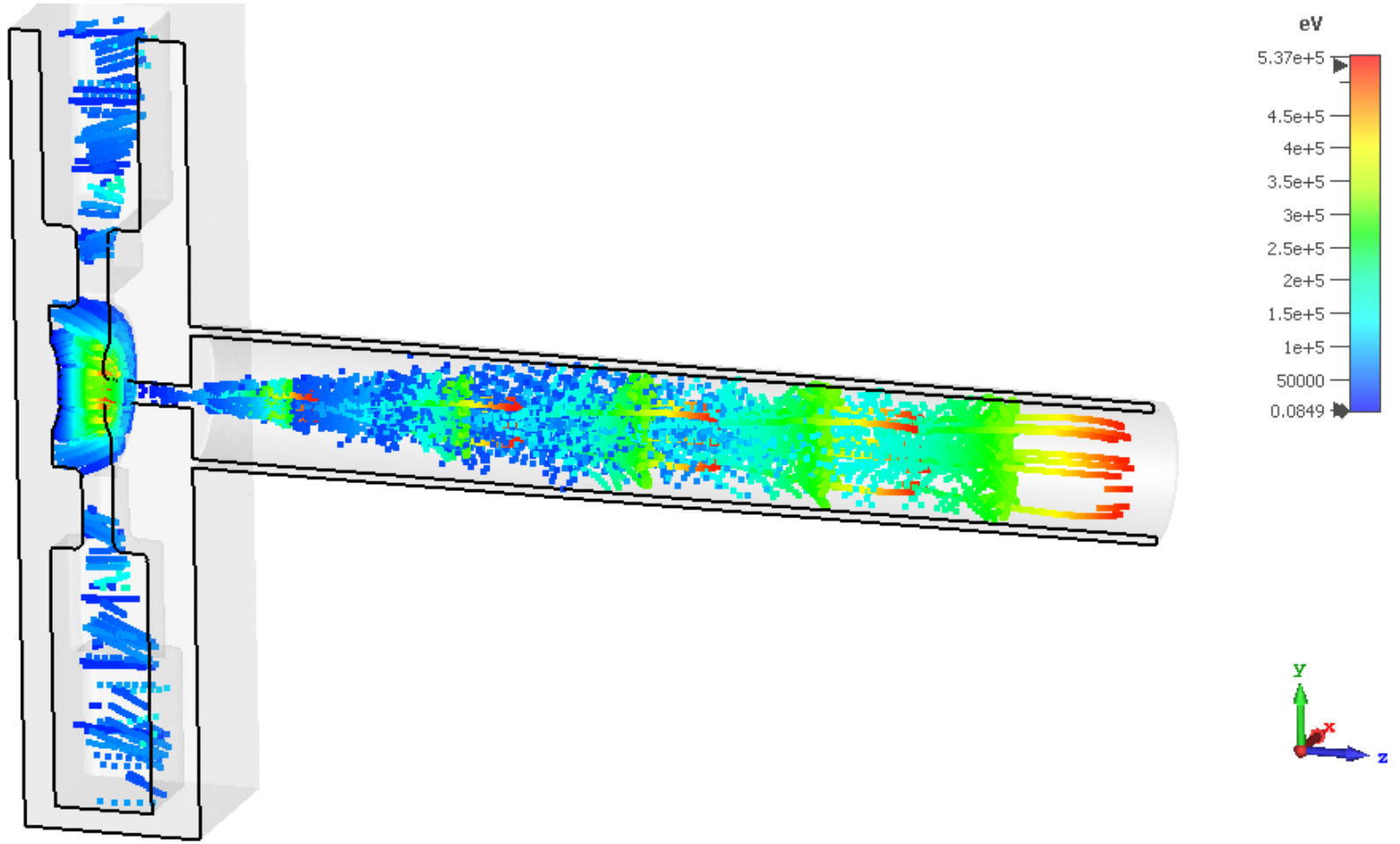

Dark current simulation

- Considering peak electric field enhancement optimized on nosecone, down stream dark current emission mostly localized to nosecone
- Isolated nosecone emission (right) showing additional collimation from iris and beam pipe

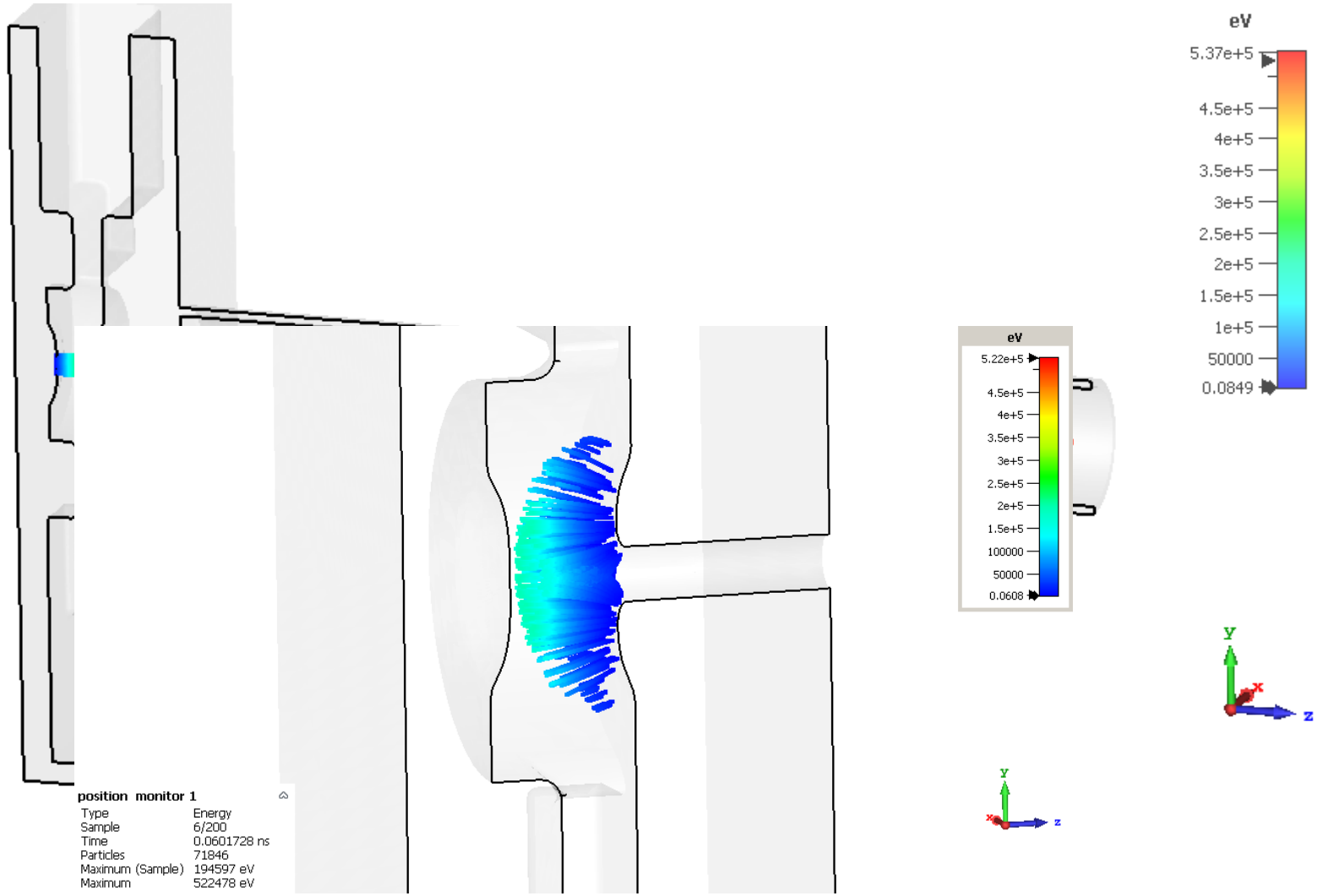

CYBORG Phase1

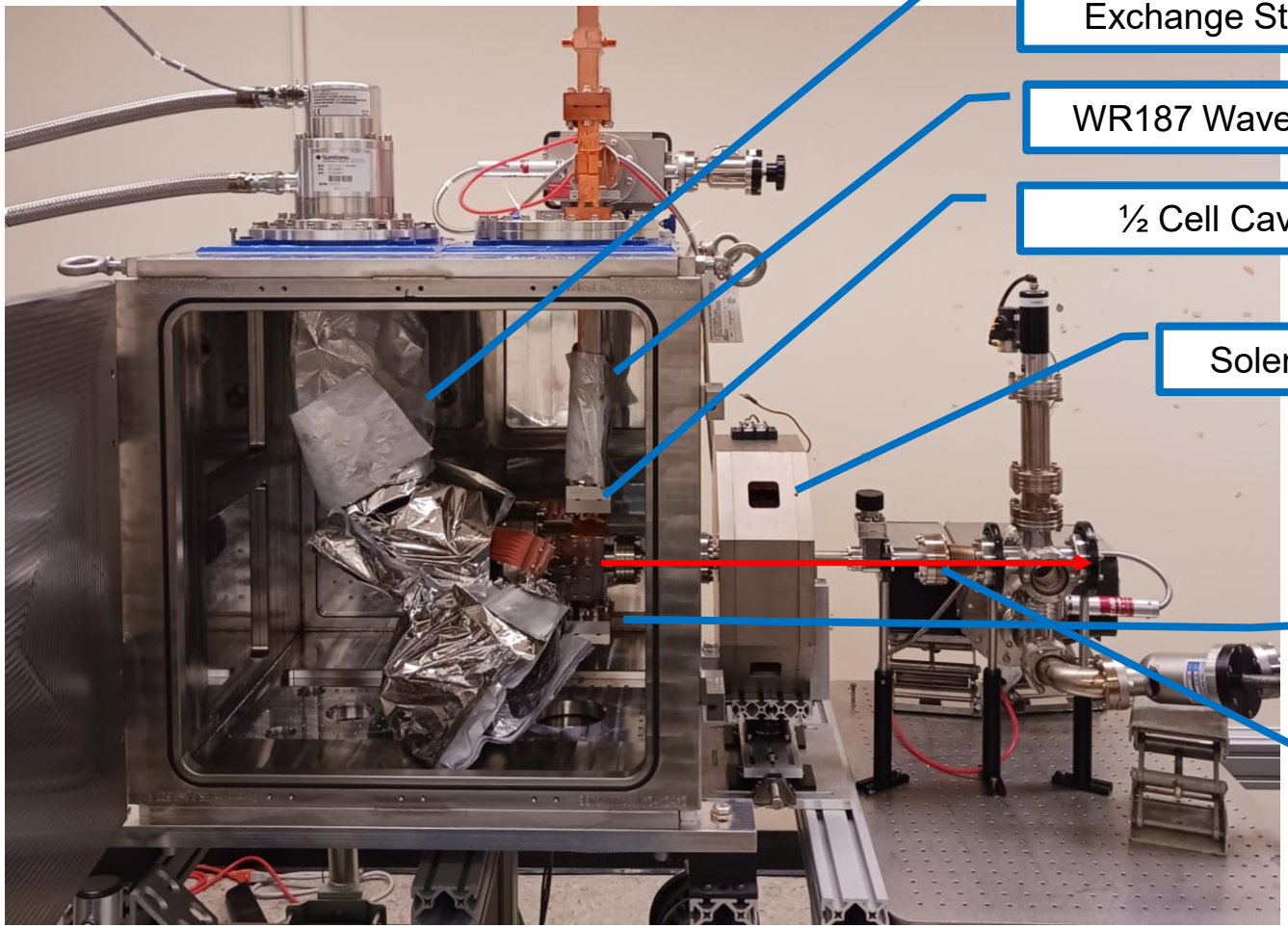

Thermal Heat Exchange Straps

WR187 Waveguide

½ Cell Cavity

Solenoid

RF Dummy port

e- beam

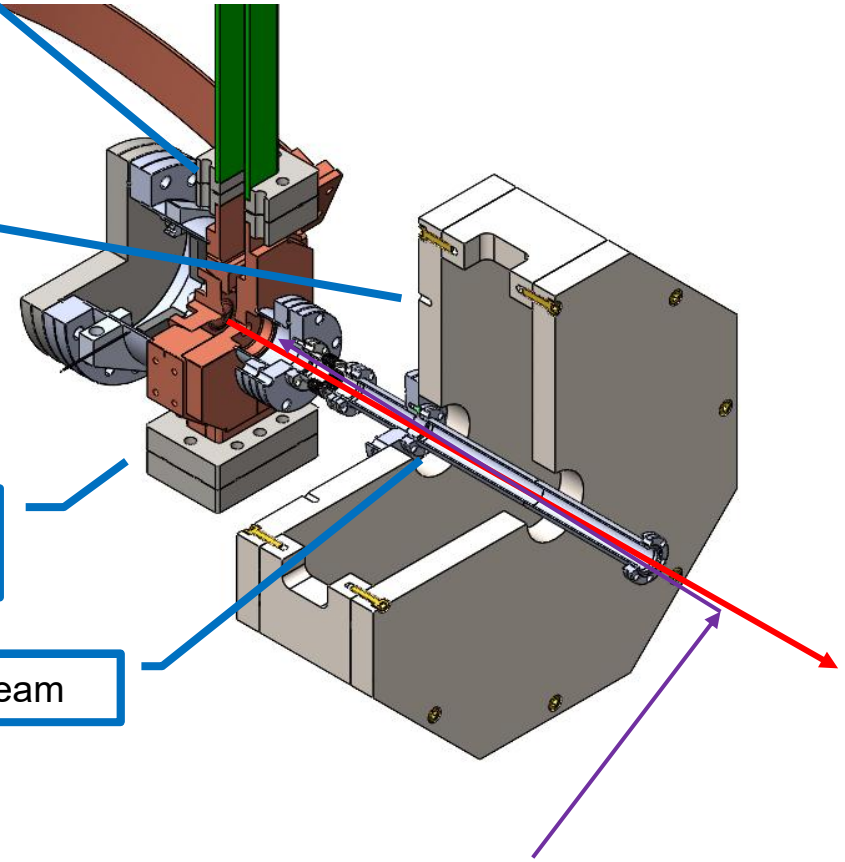

Peak RF Performance

- Maximum RF input power currently into gun between 450 – 520 kW with fluctuation, stable at 450 kW
- Max peak field estimate >90 MV/m at 85K and 78 MV/m at room temperature
  - Determined with two different methods reflected pulse QL calculation and using coupling + Q0 from low power test
- Plots below show dark current scaling which show significant improvement of field possible using same input RF power
- YAG screen dark current measurements at approximately same input power

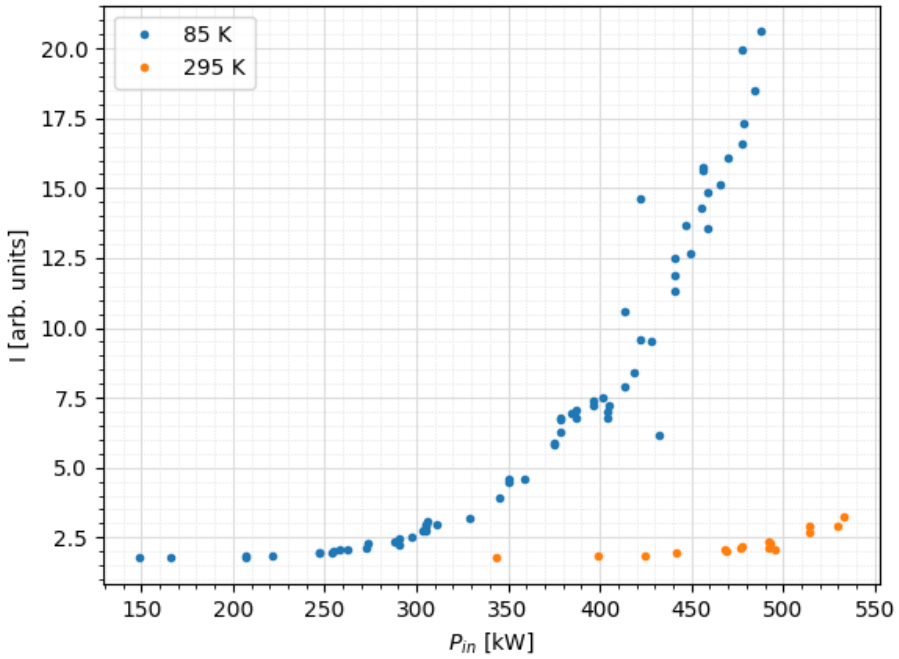

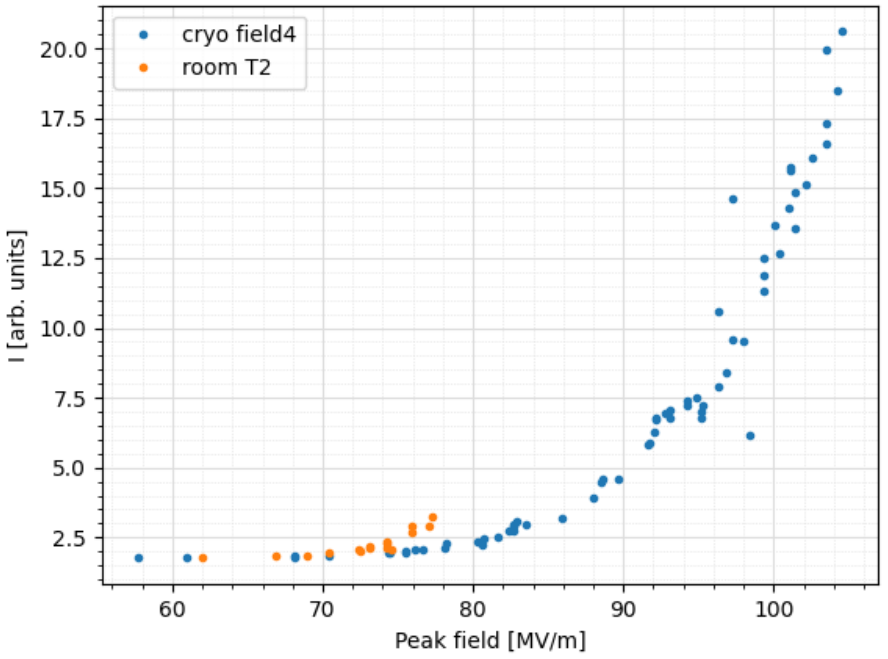

70 MV/m @ 295 K

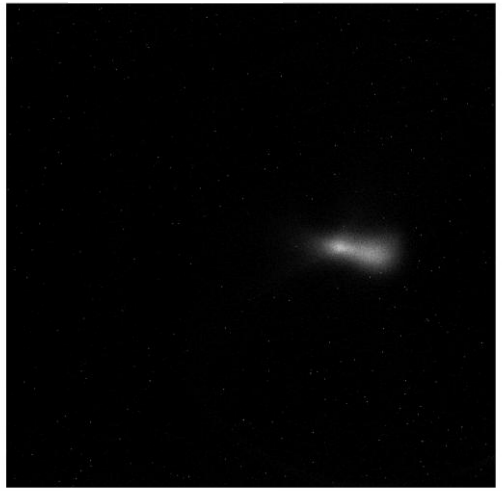

95 MV/m @ 82.5 K

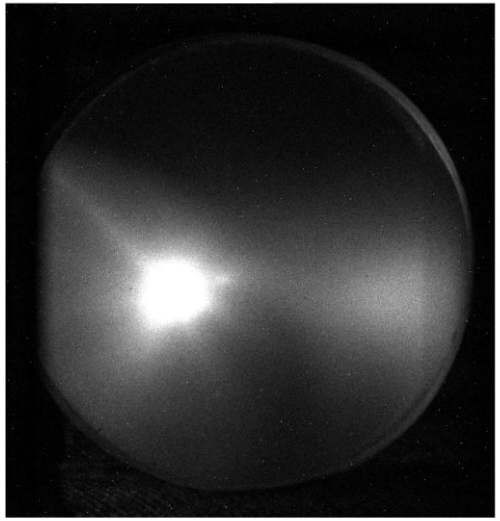

Dark current temperature dependence

- Cryogenic pulsed DC experiments show temperature dependence (below)
- Begun to see similar results in CYBORG during high field conditioning (right)

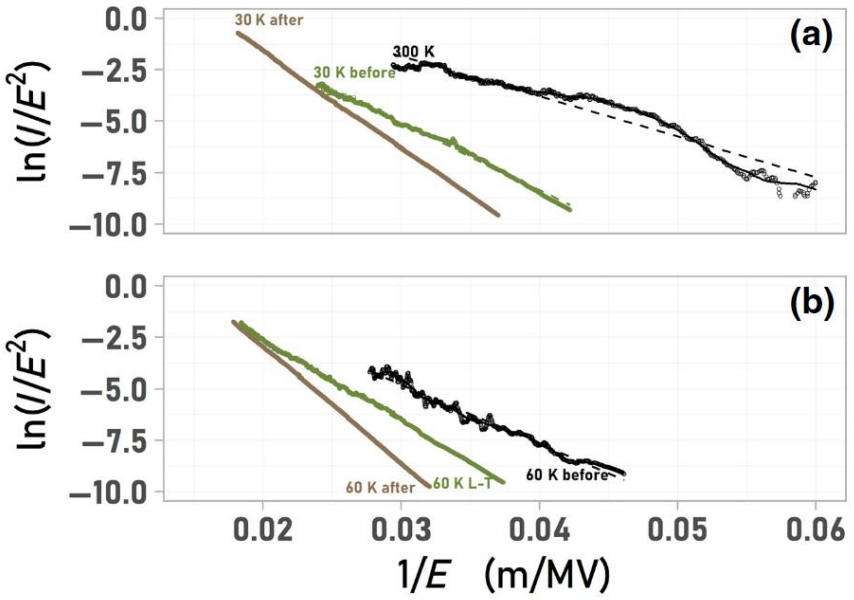

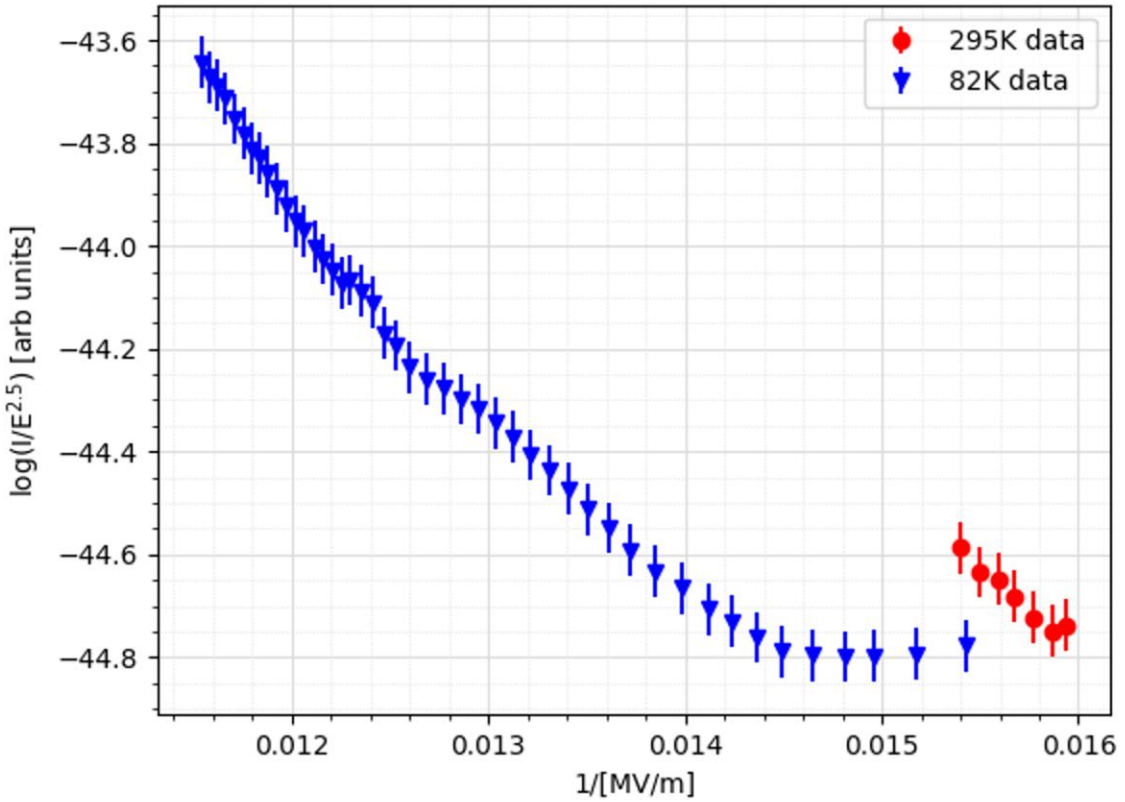

Jacewicz, Marek, et al. "Temperature-dependent field emission and breakdown measurements using a pulsed high-voltage cryosystem." *Physical Review Applied* 14.6 (2020): 061002.

Dark current temperature dependence

- Effective enhancement appears reduced for higher fields
- Data has implicit time dependence on scale of hours at 1 Hz rep rate so may represent also an effect of conditioning
- More data needed

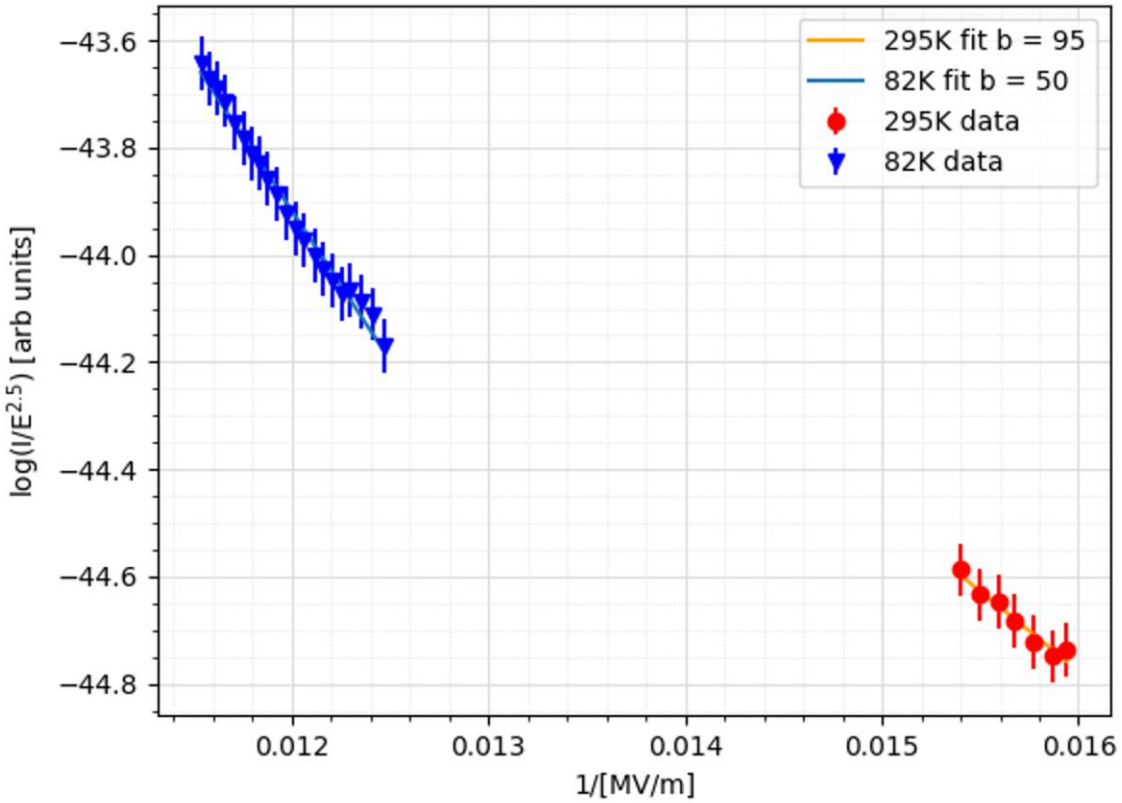

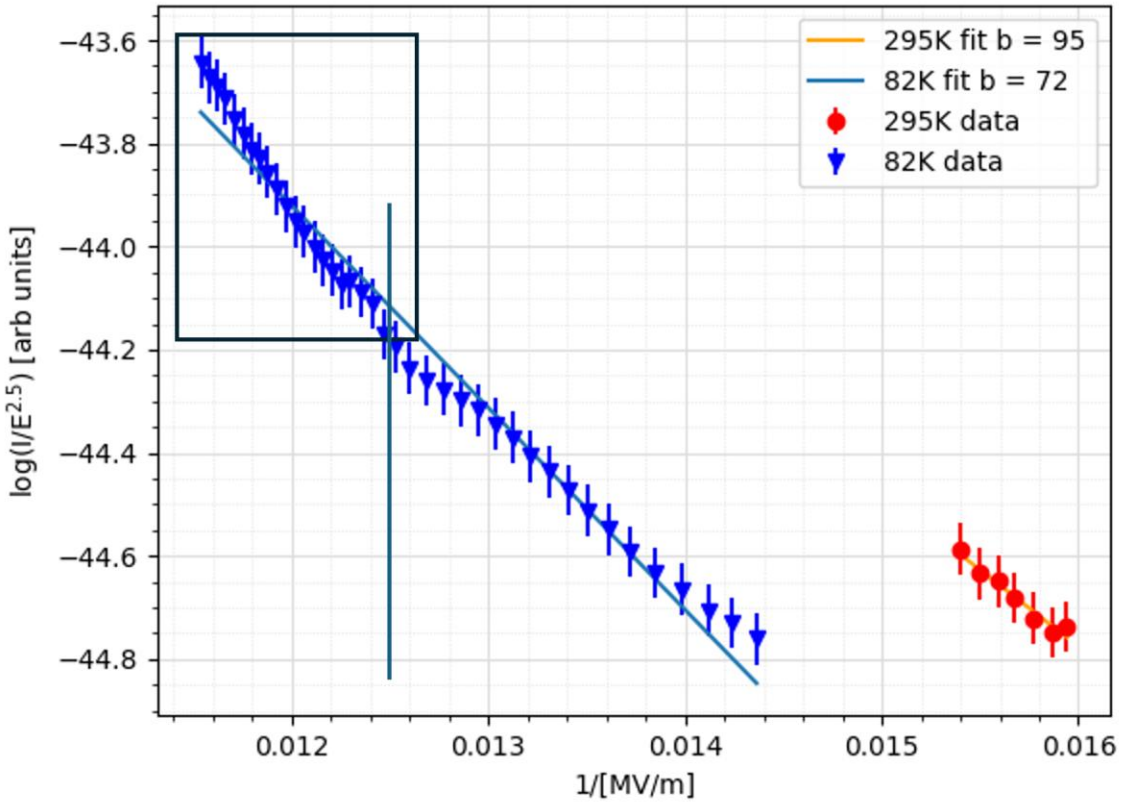

Dark current temperature dependence

- Effective enhancement appears reduced for higher fields
- Data has implicit time dependence on scale of hours at 1 Hz rep rate so may represent also an effect of conditioning
- More data needed

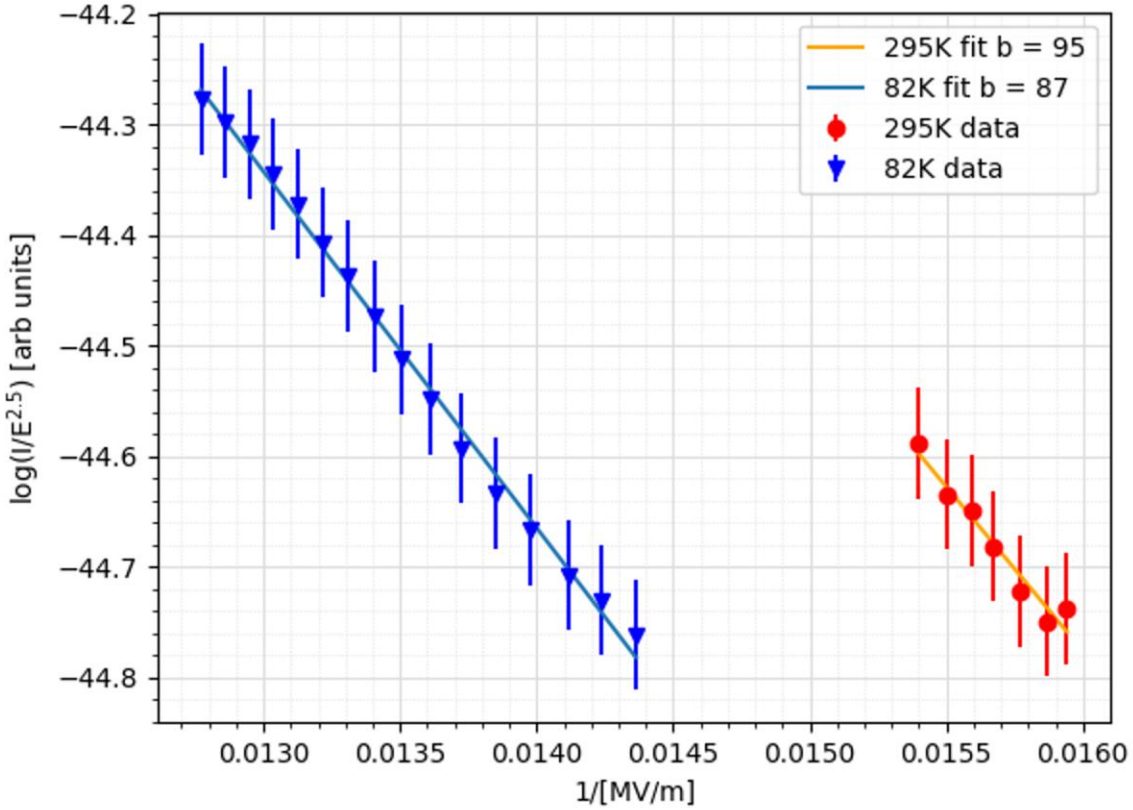

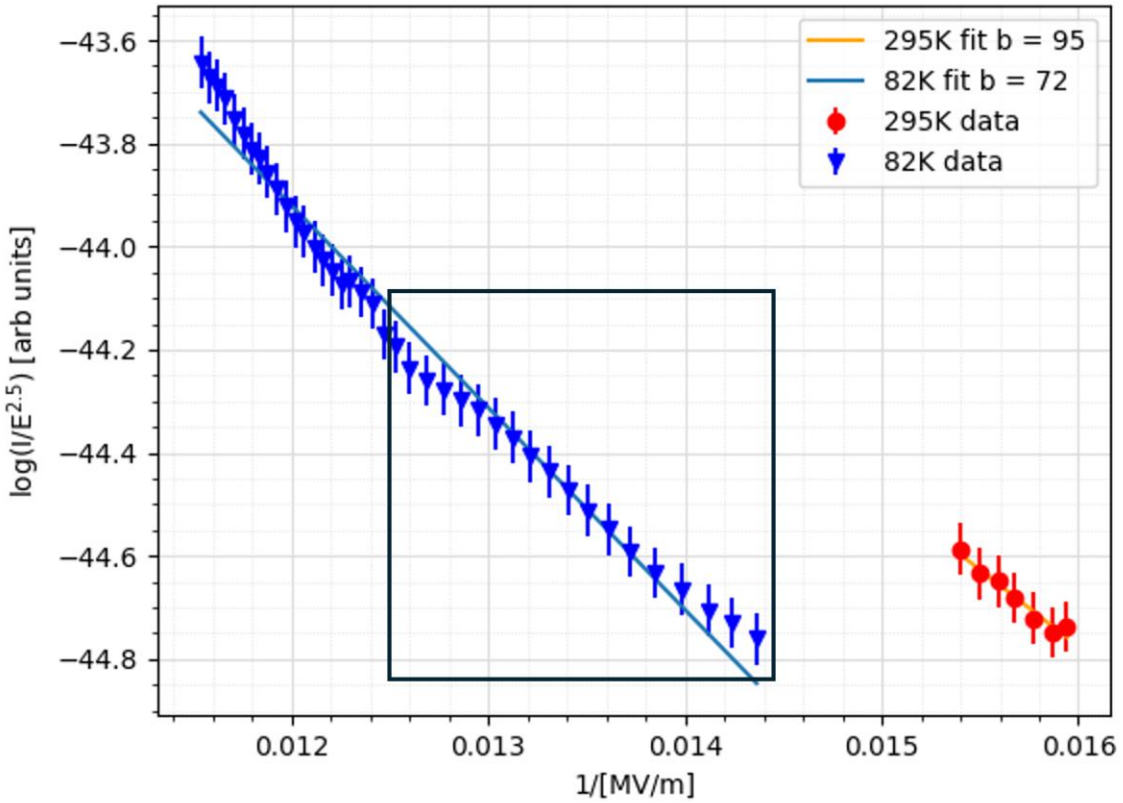

Cryogenic Dark Current

- Approximate total charge can be estimated via *beam loading* i.e. measured loss in Q0 from expected values in presence of excess charge giving approx. 10s pC
- From additional PIC simulation analysis, 7-8% of electrons make it >30 cm downstream, so < 1 pC expected downstream (25+ cm)
- 10-100 pC/2 us = 5-50 uA total and 0.5 pC expected downstream
- 500 uA in LCLS, 50 uA in SwissFEL, 10 uA in superconducting EuXFEL (2 m downstream)

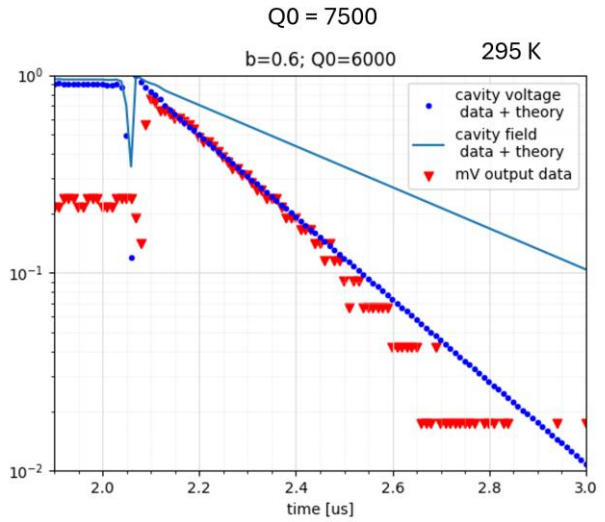

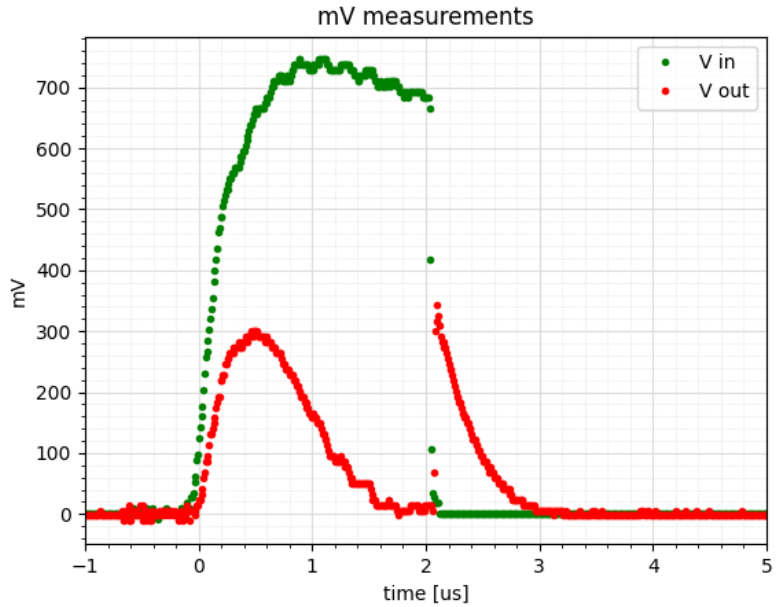

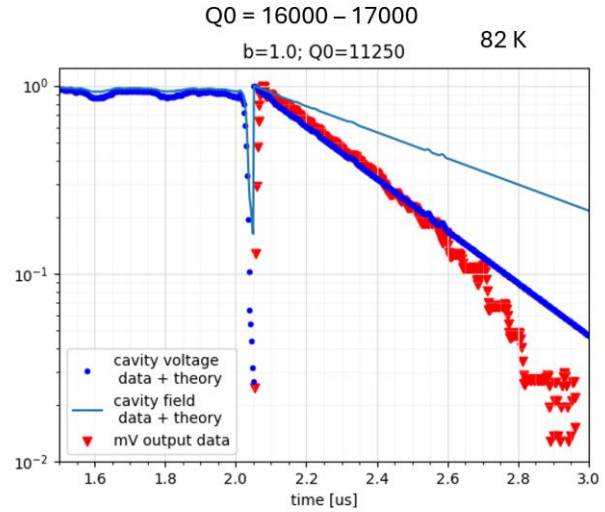

G. Shu et al, *Nuclear Instruments and Methods in Physics Research Section A: Accelerators, Spectrometers, Detectors and Associated Equipment*, Volume 1010, 2021,165546, ISSN 0168-9002, doi:10.1016/j.nima.2021.165546.

GTF emission

- Rather than Fowler –Nordheim for completeness use a general thermal-field emission model via Jensen that incorporates thermionic and field emission contributions

$$J_{GTF}(F,T) = \begin{cases} n^{-2}J_F + J_T & (n < 1) \\ J_F + n^2 J_T & (n > 1) \end{cases}$$

Jensen, Kevin L., and Marc Cahay. "General thermal-field emission equation." *Applied physics letters* 88.15 (2006).

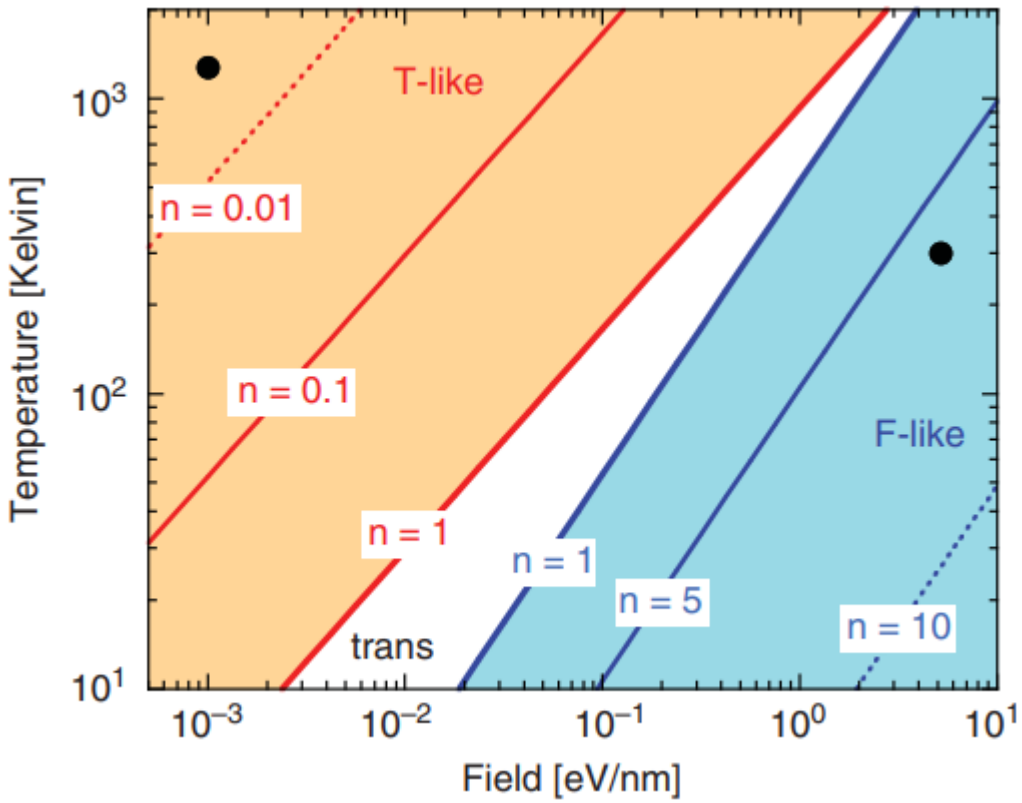

Jensen, Kevin L. *Introduction to the physics of electron emission*. John Wiley & Sons, 2017.

GTF emission

- Rather than Fowler –Nordheim for completeness use a general thermal-field emission model via Jensen that incorporates thermionic and field emission contributions

$$J_{GTF}(F,T) = \begin{cases} n^{-2}J_F + J_T & (n < 1) \\ J_F + n^2 J_T & (n > 1) \end{cases}$$

Jensen, Kevin L., and Marc Cahay. "General thermal-field emission equation." *Applied physics letters* 88.15 (2006).

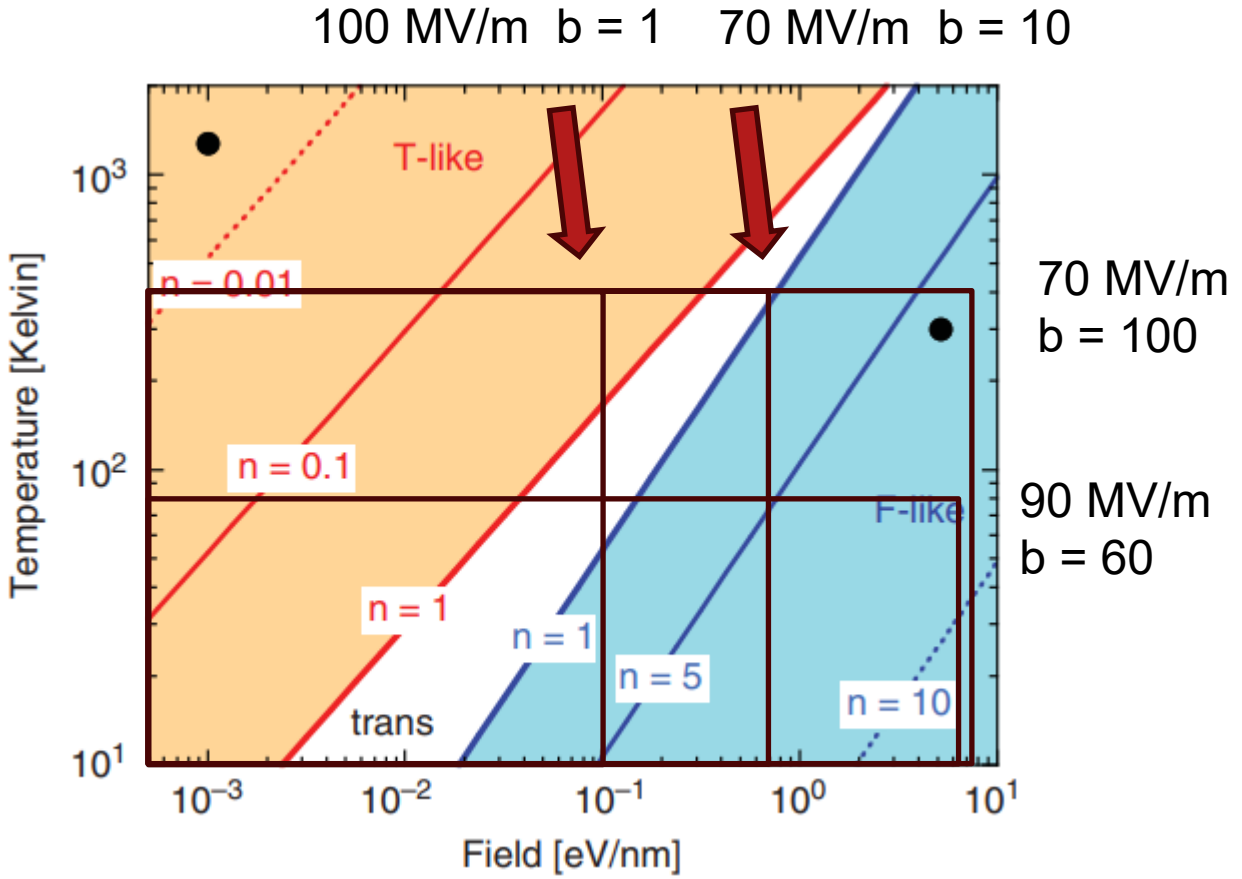

Jensen, Kevin L. *Introduction to the physics of electron emission*. John Wiley & Sons, 2017.

GTF emission

- Pulse heating needed to achieve some reasonable visible effect (400 K)
- But Cu melts at certain temperatures
- Scaling similar to BDR in high gradient regime, E^30 (below)

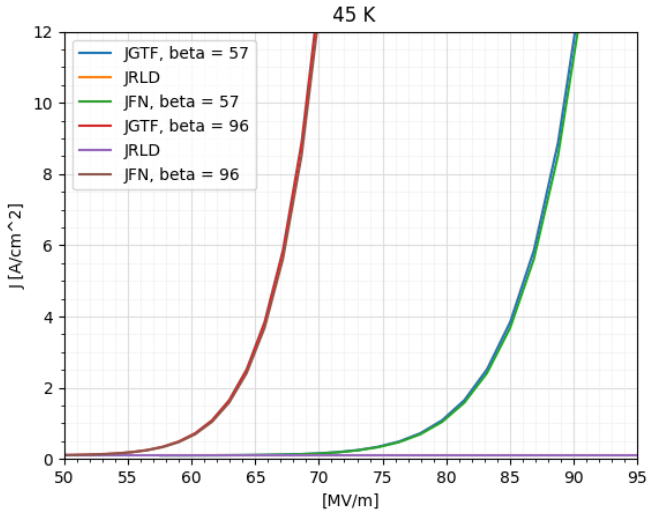

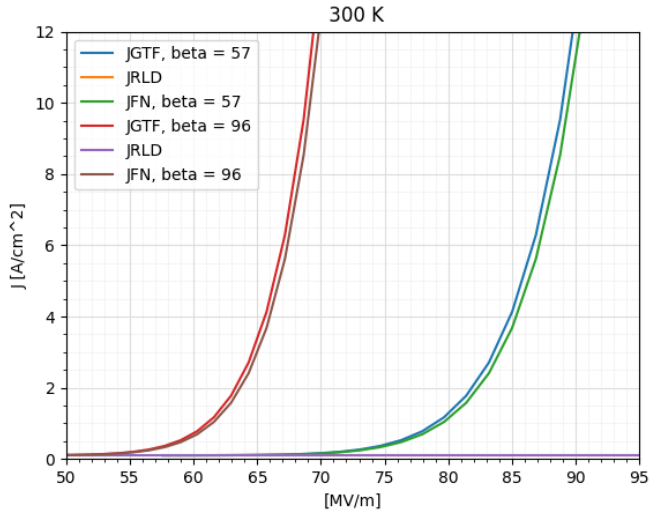

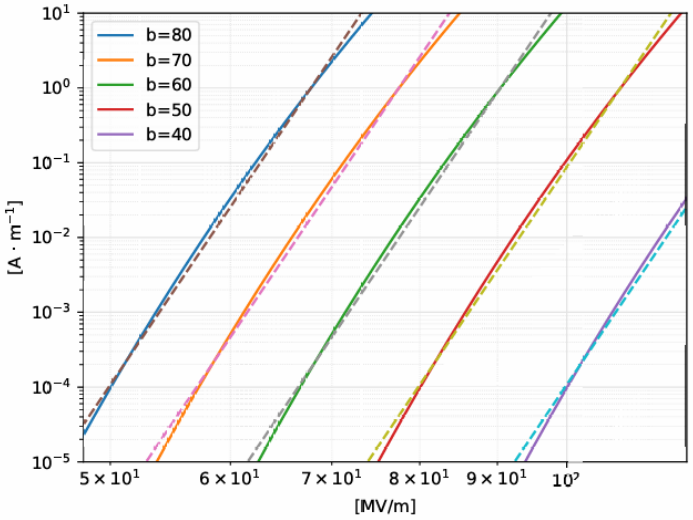

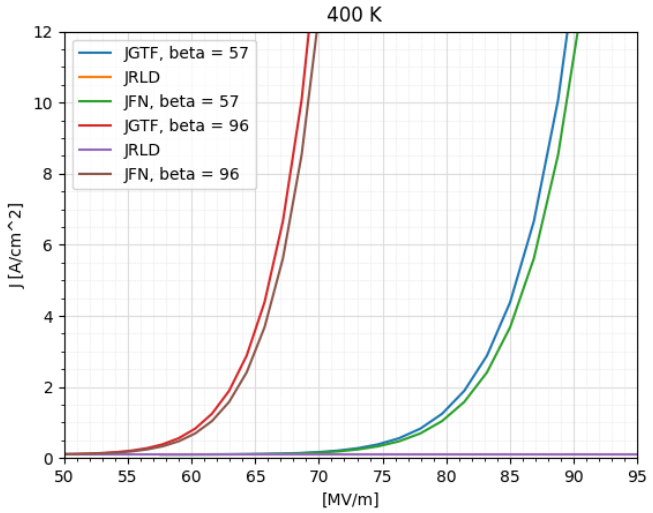

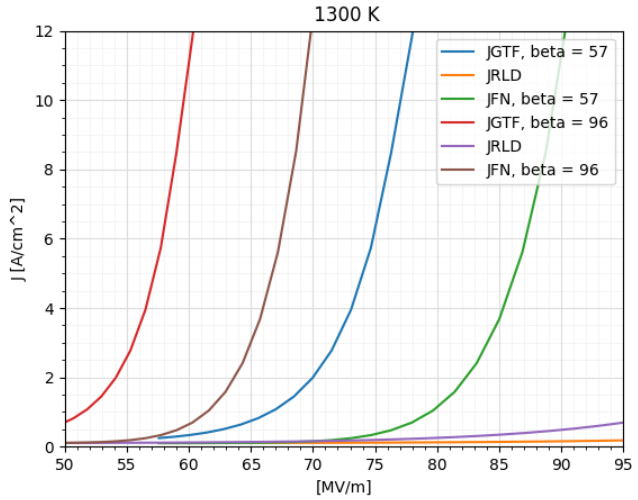

Emission tip model

- Temperature dependence not present in Fowler-Nordheim tunneling
- Useful simple model, taking effective β, and scaling field to get geometric deformation empirically to obtain room temperature value
- Then using NIST Young's modulus and Poisson ratio for copper to obtain reduced field enhancement geometry at low temperatures due to increased material hardness

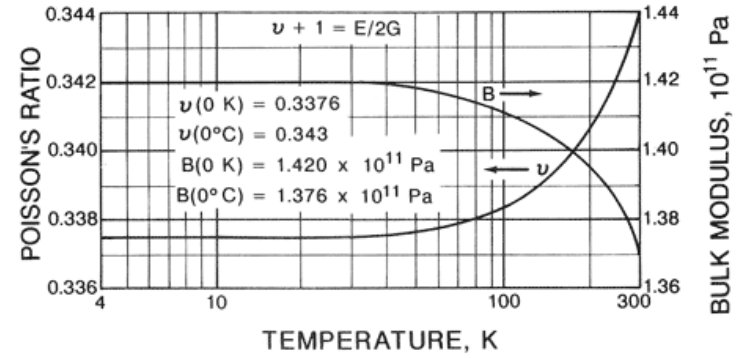

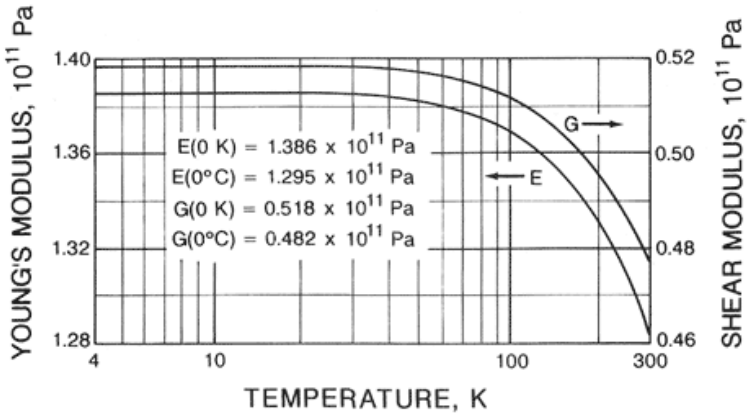

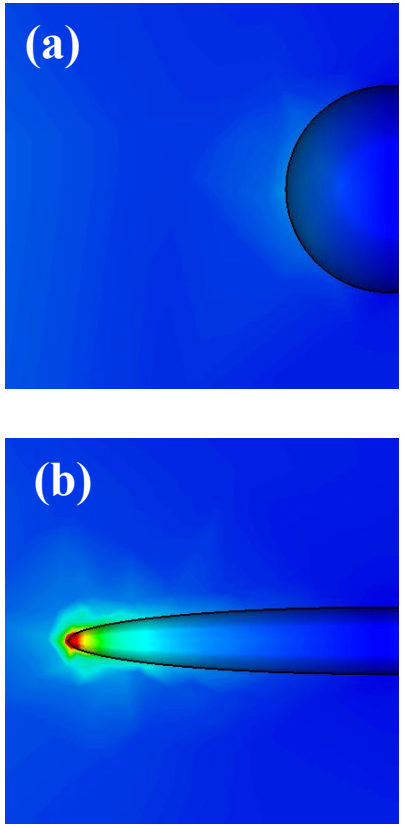

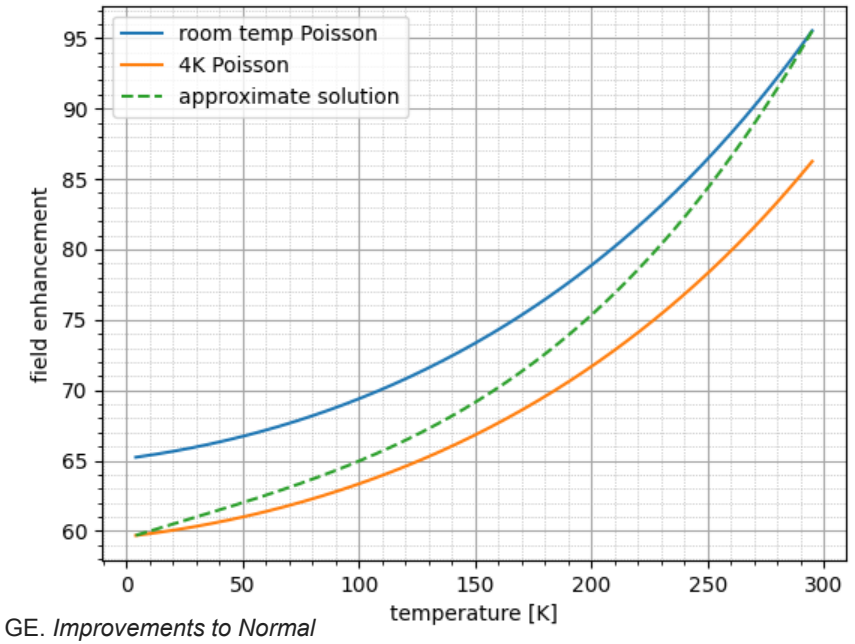

Lawler, GE. *Improvements to Normal Conducting High Gradient Accelerator Performance at Cryogenic Temperatures*. University of California, Los Angeles, 2024.

RF heating contribution

- Main gun section shown outside of cryostat (far left)
- Simplified thermal steady state simulation shown (middle) with previous cooling configuration to show accuracy of transient cooling simulations given estimated heat leaks from waveguide, beam pipe etc.
- RF heating over 6 hours (right) at 1 Hz ≈ 0.8 W

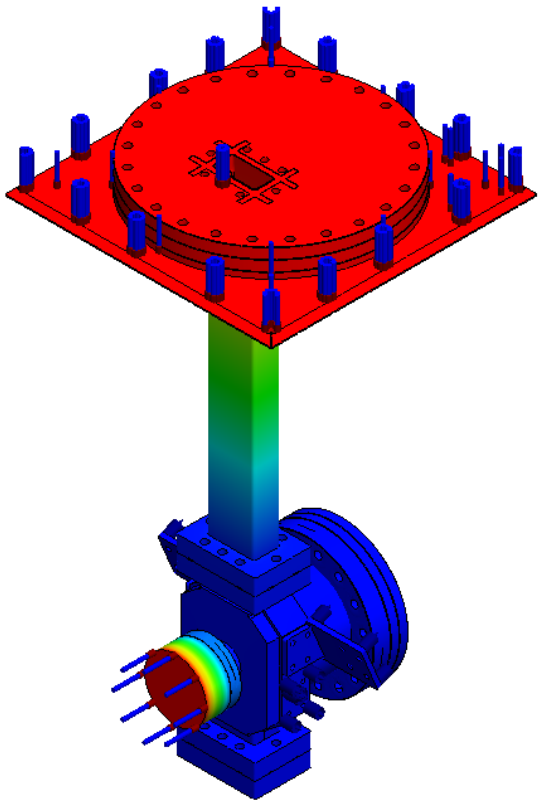

$$\Delta T(T) = \frac{R_s(T)\left|H_{||}\right|^2\sqrt{t}}{\sqrt{\pi\rho' c_\epsilon \sigma LT}} \propto \frac{R_s(T)}{\sqrt{\rho' c_\epsilon \sigma LT}} \propto \frac{R_s(T)}{\sqrt{\rho' c_\epsilon \sigma T}}$$

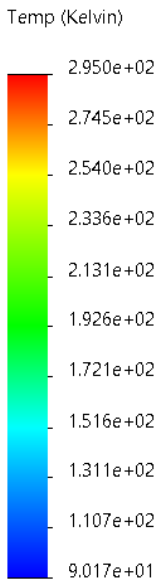

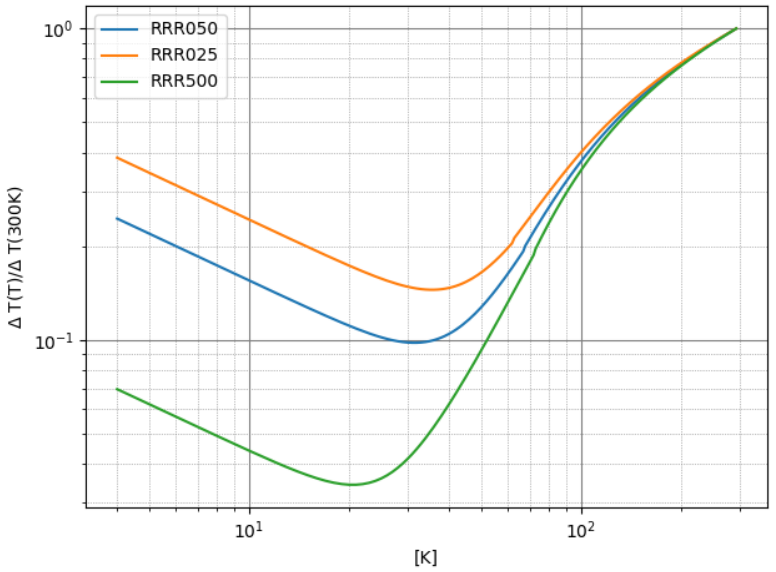

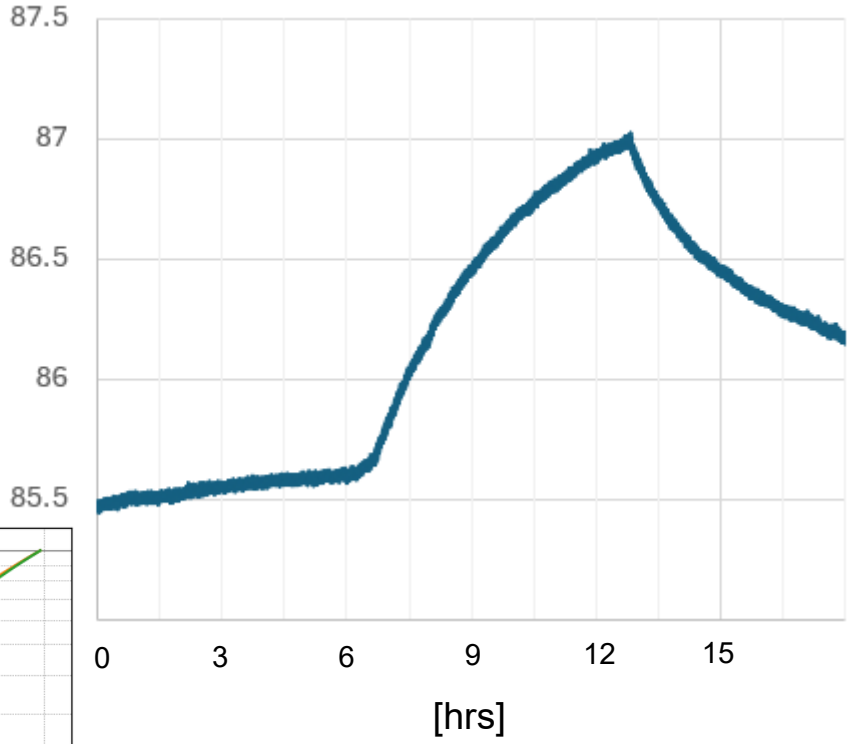

RF heating contribution

- Main gun section shown outside of cryostat (far left)
- Simplified thermal steady state simulation shown (middle) with previous cooling configuration to show accuracy of transient cooling simulations given estimated heat leaks from waveguide, beam pipe etc.
- RF heating over 6 hours (right) at 1 Hz ≈ 0.8 W

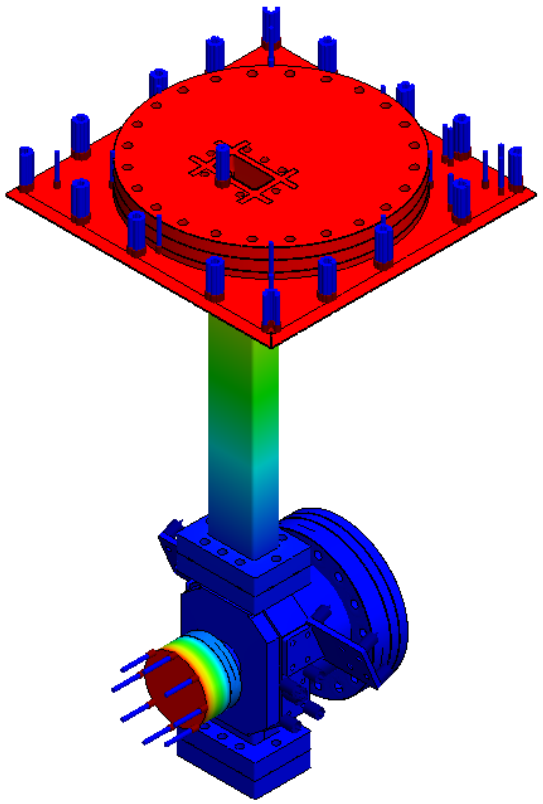

$$\Delta T(T) = \frac{R_s(T)\left|H_{||}\right|^2\sqrt{t}}{\sqrt{\pi\rho' c_\epsilon \sigma L T}} \propto \frac{R_s(T)}{\sqrt{\rho' c_\epsilon \sigma L T}} \propto \frac{R_s(T)}{\sqrt{\rho' c_\epsilon \sigma T}}$$

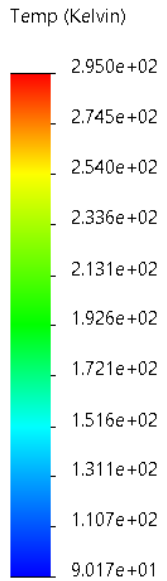

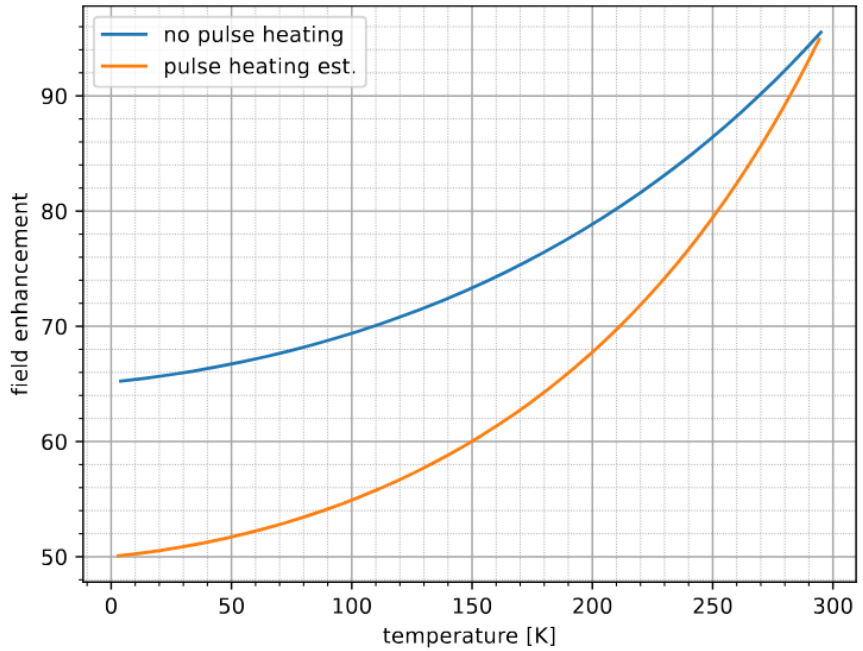

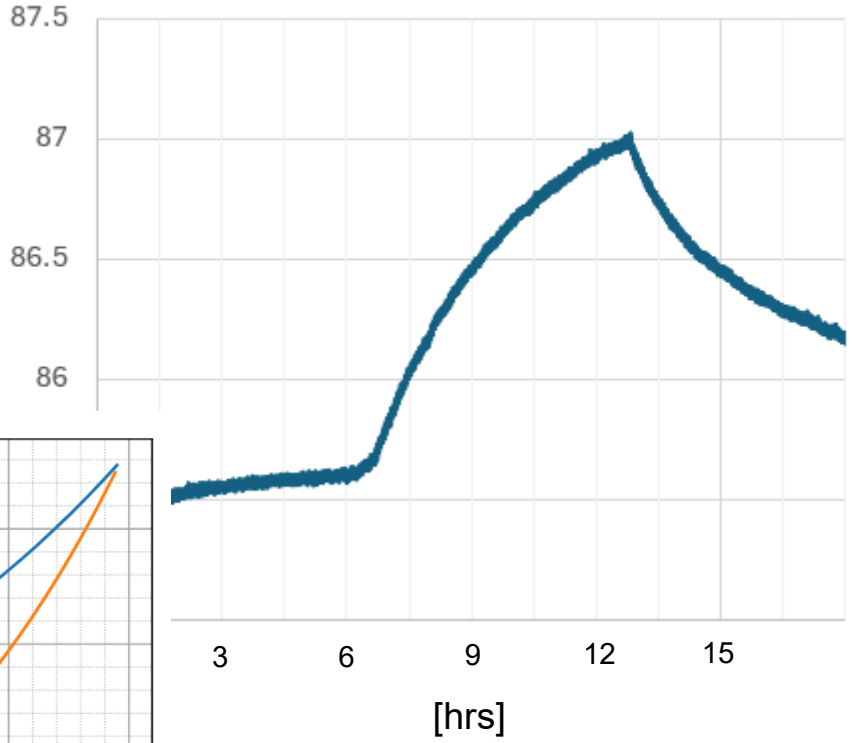

Temperature dependent RF resistance

- Surface resistance minimum at cryogenic temperatures measured for samples in SLAC mushroom dome cavity
- Plotted for various RRR (right)

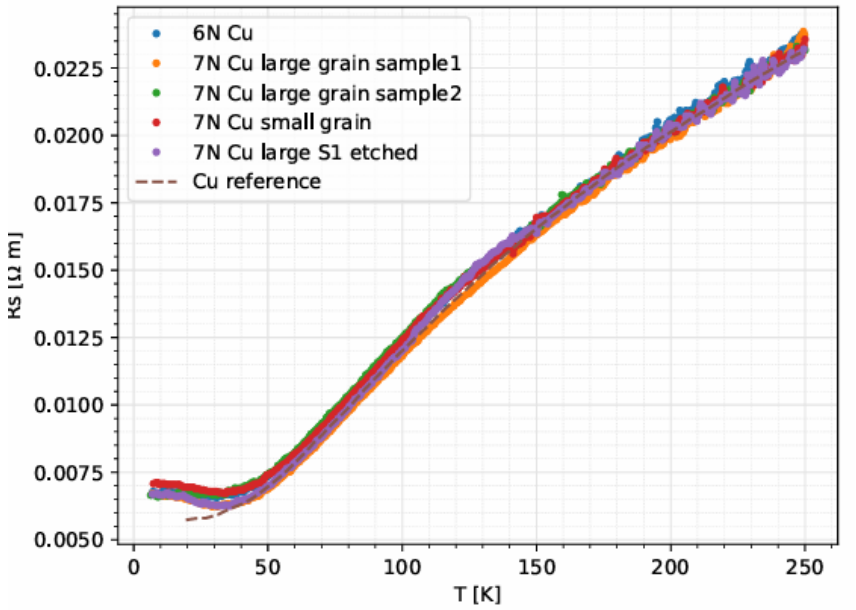

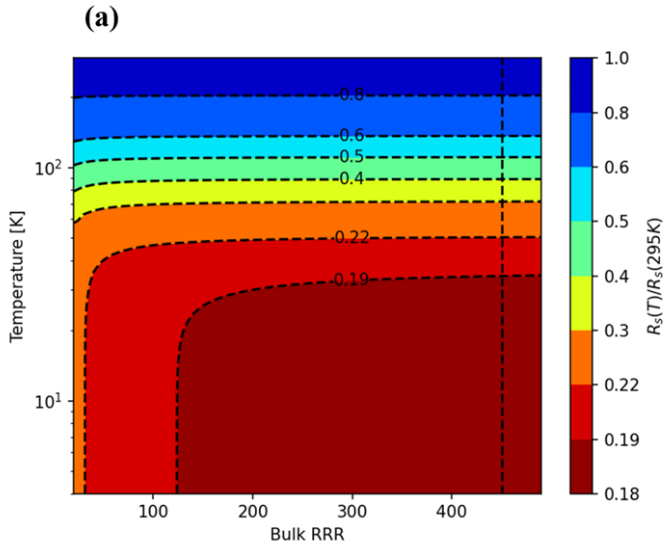

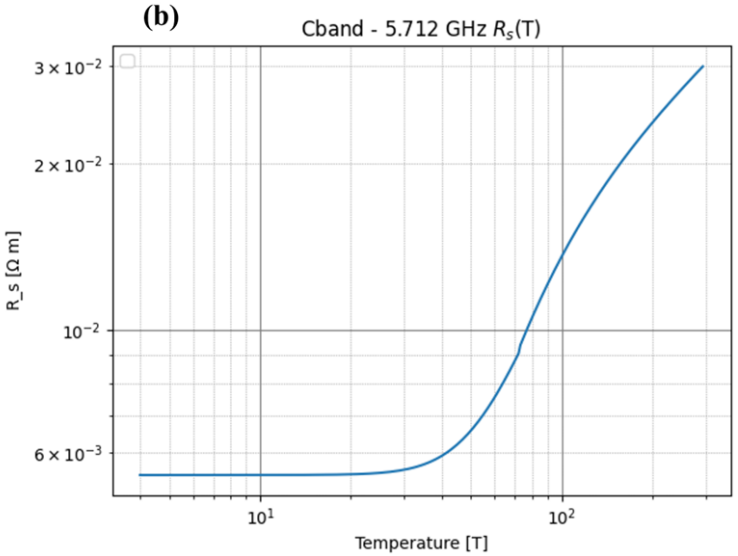

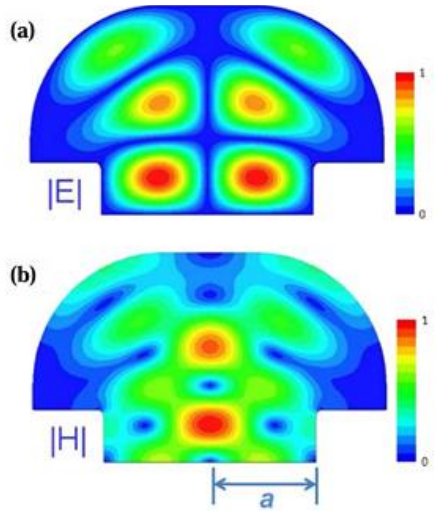

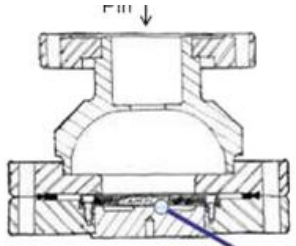

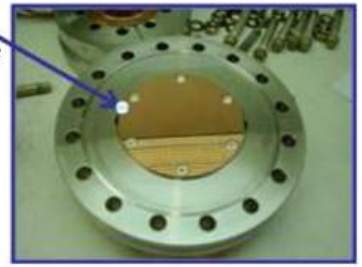

3-inch diam. pulse heating sample

Laurent, Lisa, et al. "Experimental study of rf pulsed heating." *Physical Review Special Topics—Accelerators and Beams* 14.4 (2011): 041001.

Thin film model

- Thin film explanation via theory of Gurzhi which found local minimum in surface resistance at cryo

R. Gurzhi, “Contribution to the theory of the skin effect in metals at low temperatures,” Sov. Phys. JETP, vol. 20, pp. 1228–1230, 1964.

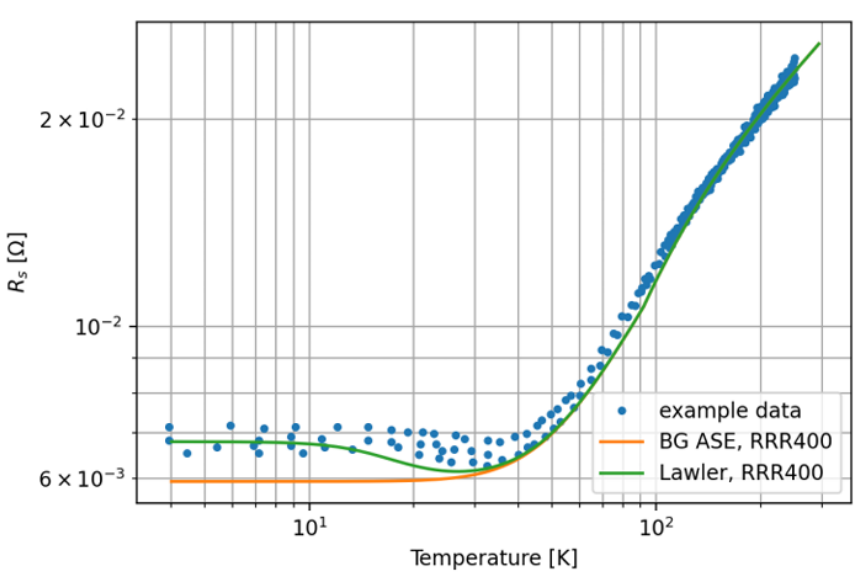

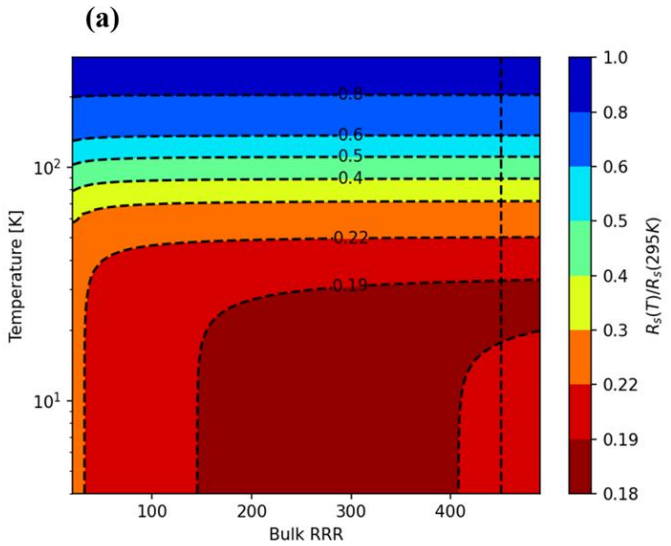

Lawler, Gerard, Fabio Bosco, and James Rosenzweig. "Improving interface physics understanding in high-frequency cryogenic normal conducting cavities." *arXiv preprint arXiv:2310.11578* (2023).

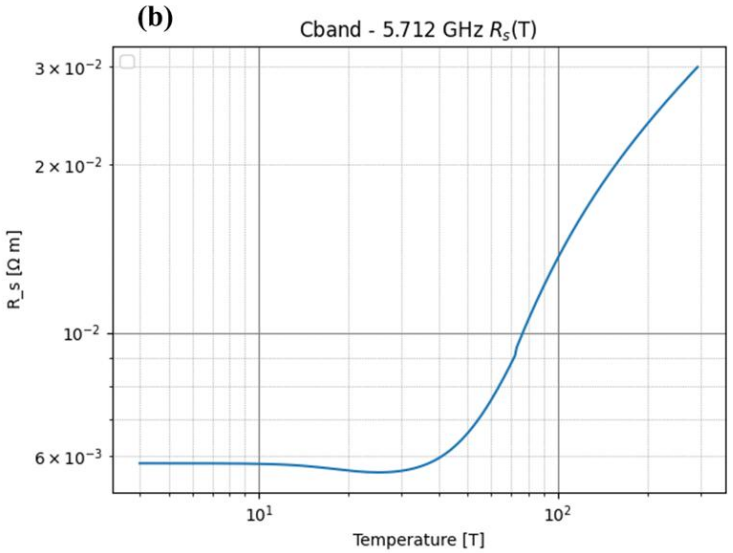

Polini, Marco, and Andre K. Geim. "Viscous electron fluids." *Physics Today* 73.6 (2020): 28-34.

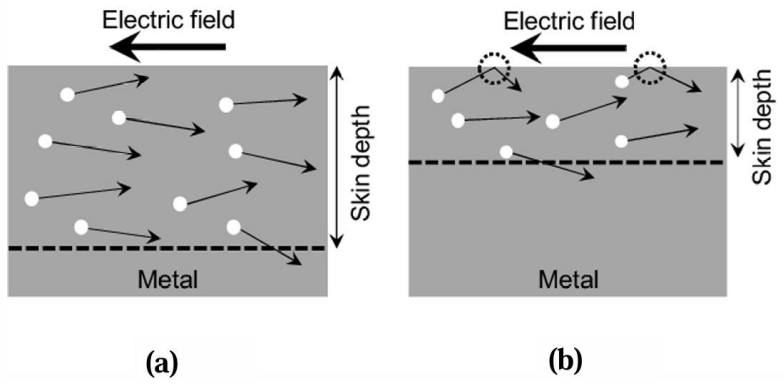

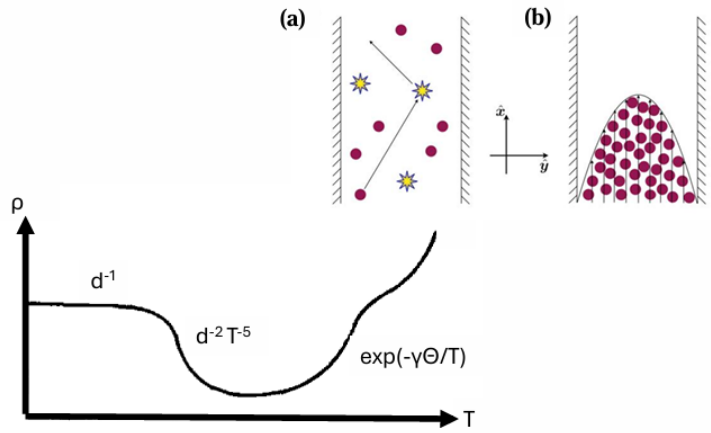

Thin film implications

- in ASE regime for Cband for examples drops into 10s nm
- Thin film behavior may lead to more semiconductor like behavior leading to temperature changes have a greater consequence
- Field emitted current as function of inverse field example (right) from Jensen demonstrating qualitatively reduced value as temperature goes down
- Cryogenic temperature extension needed

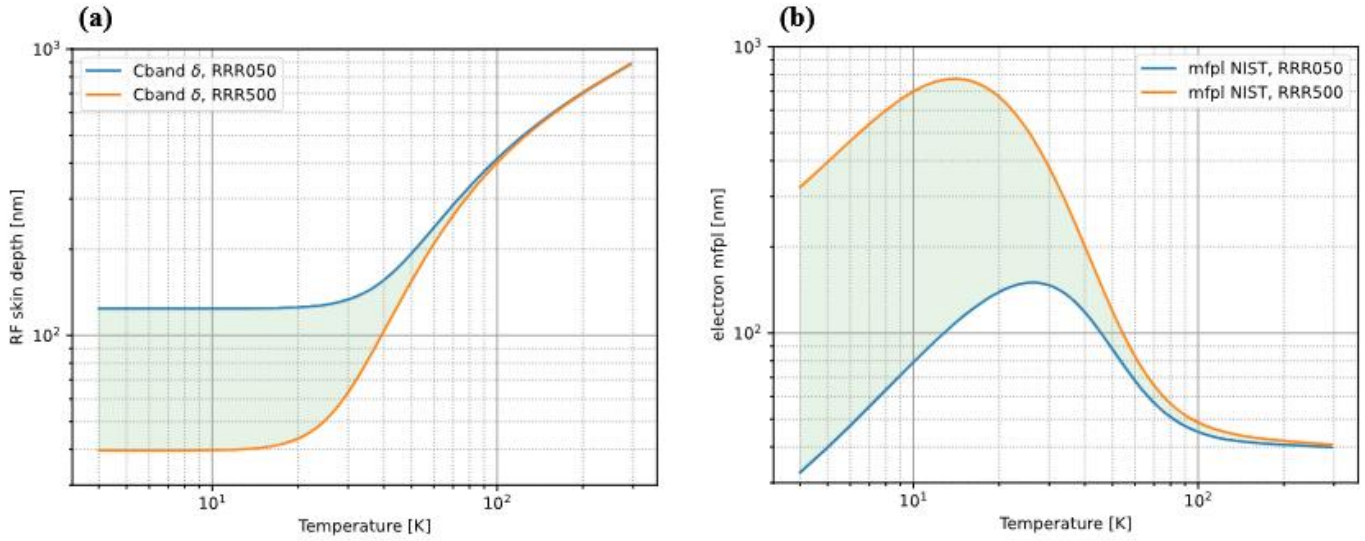

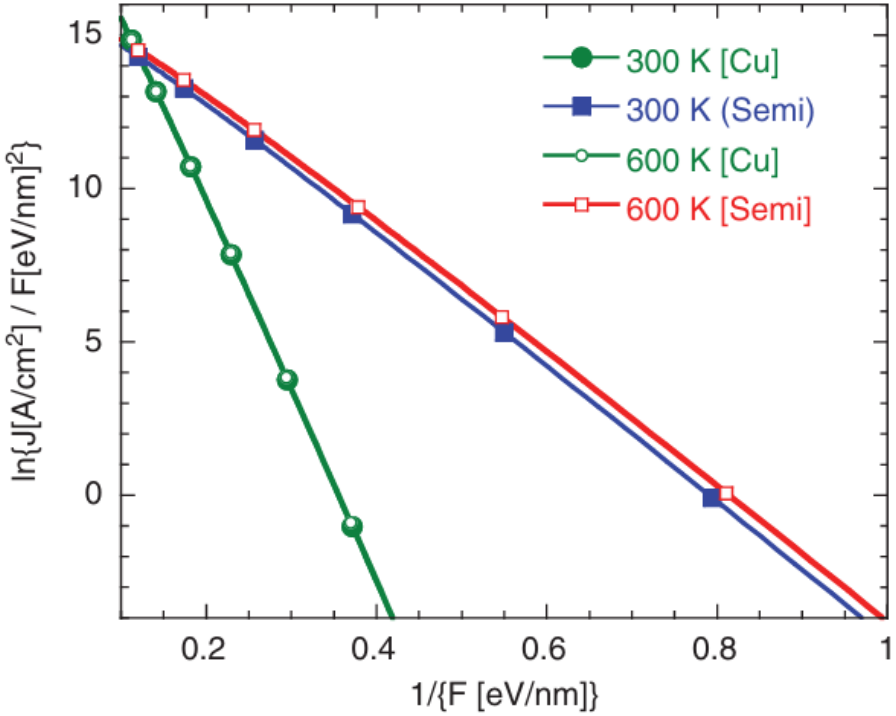

Jensen, Kevin L. *Introduction to the physics of electron emission*. John Wiley & Sons, 2017.

Multiobjective optimizations for UED

(a)

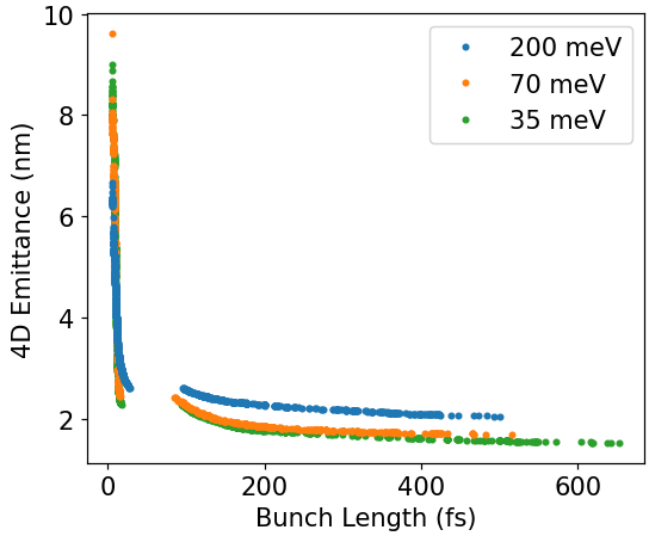

(b)

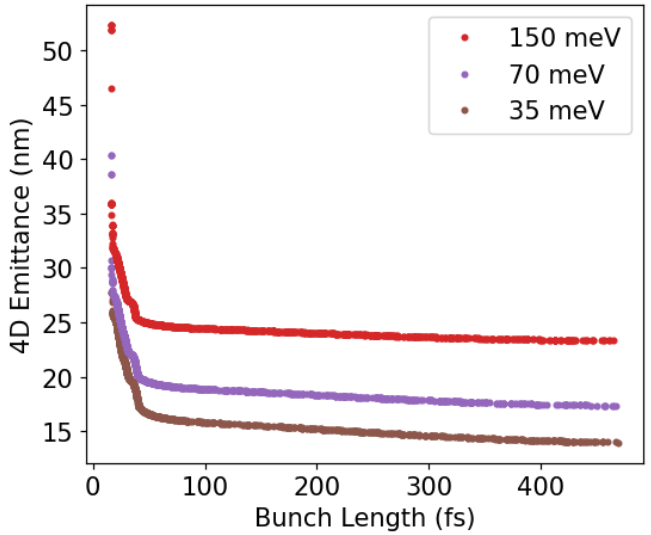

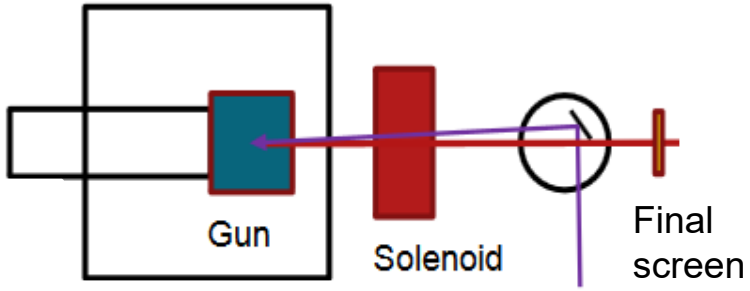

Variables	Range
Gun phase offset ($\Delta\phi$)	[-10, 10] degrees (ϕ_0 = 125 deg)
Solenoid position	[0.24, 0.6] m
Sol strength	[0.0, 3.0] (0.95-> ~0.13 T)
Initial bunch length	[50, 300] fs

Constants	Value
Charge	16 fC
Peak field	180 MV/m
Screen (sample)	1.5 m
Spot size at cathode	(a) 1.2 μm (b) 40.0 μm

Phase2 Load lock

- Difficulty of interference fit for cathode coupling not reliable in near term
- Shift to knife edge coupling with sufficiently thermally isolated transfer arm

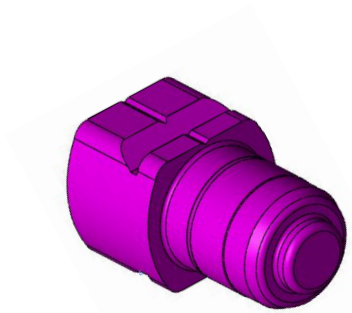

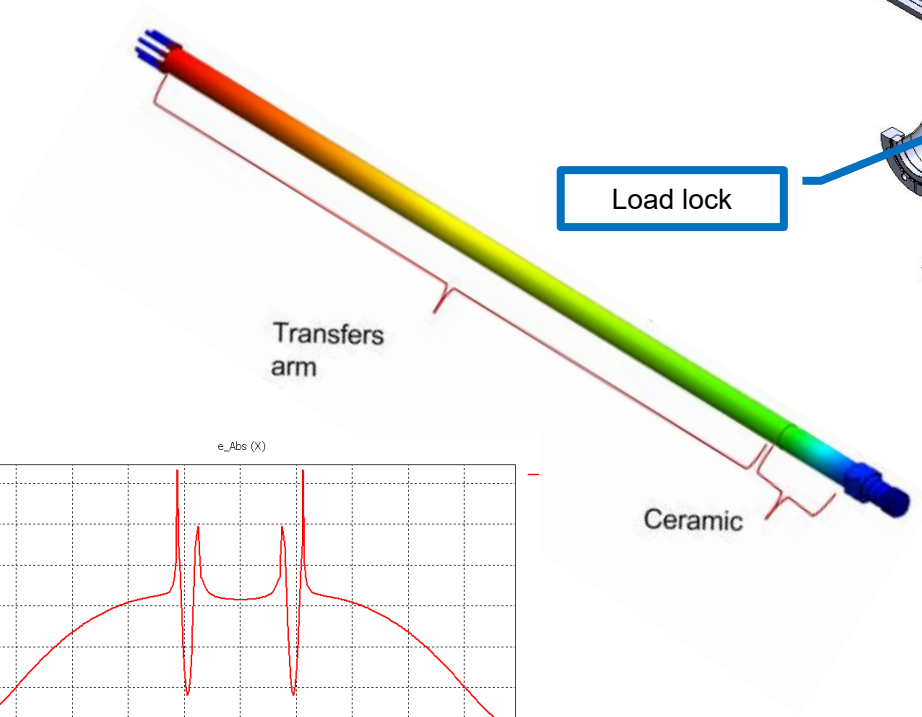

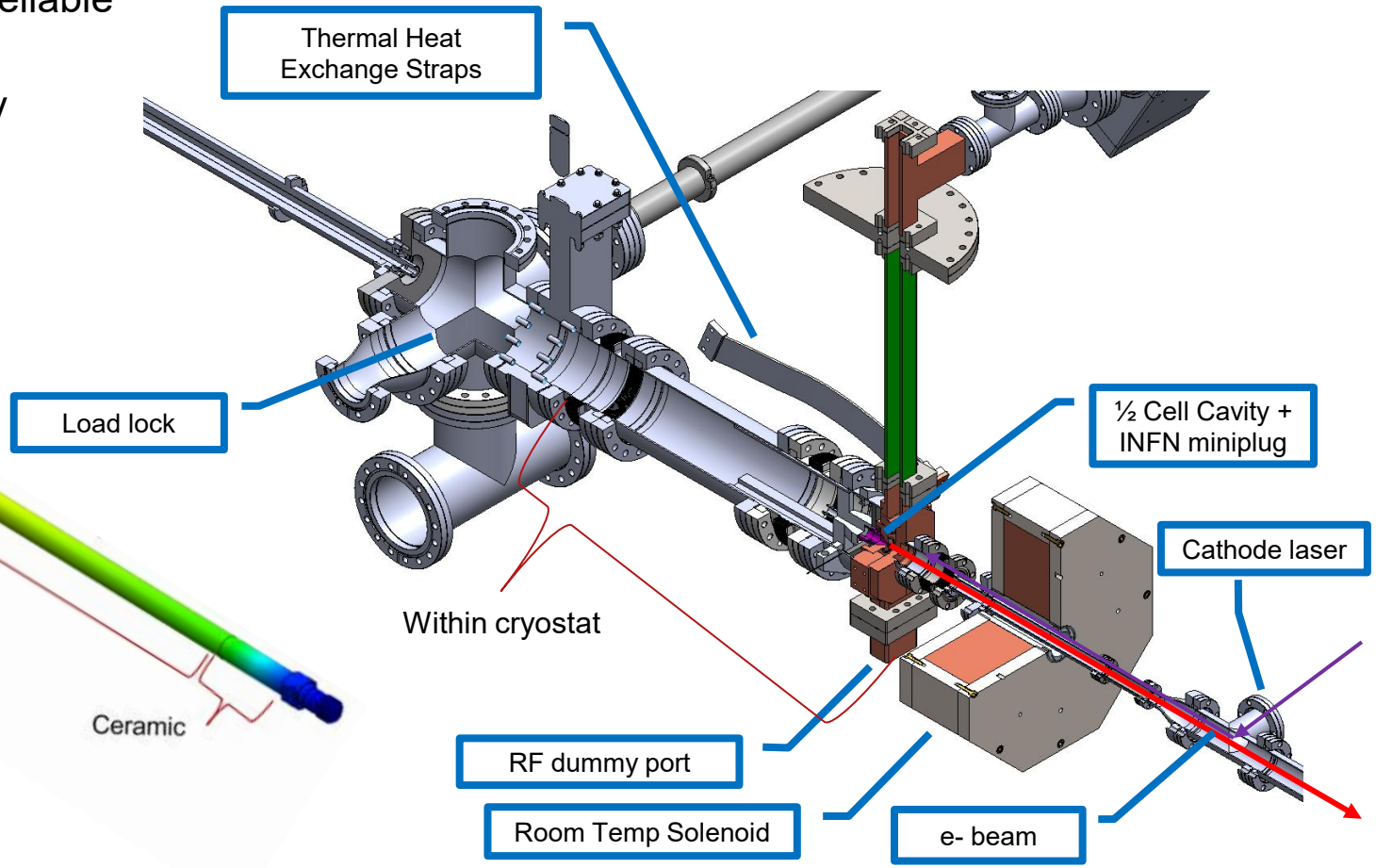

5. Conclusions

1. High gradient cavities here means BDR reduced meaning cryogenic and/or heating minimized leads to increasing consideration of dark current needed
2. Empirical cryogenic reduction could be advantageous for high gradient brightness operation complementary to BDR reduction alone
3. Physics of emission at cryogenic temperatures complex and interesting
4. Capabilities to study increasing significantly at UCLA and LANL

5. Conclusions

- Fabio Bosco, Obed Camacho, Atsushi Fukasawa, David Garcia, *Richard Li,* Pietro Musumeci, Brian Naranjo, Pratik Manwani, Jake Parsons, *April Smith, Sean O'Tool,* Yusuke Sakai, Oliver Williams, Monika Yadav
- Paul Carriere, Nanda Matavalam
- Evgenya Simakov, Anna Alexander, Petr Anisimov, Haoran Xu
- Martina Carillo, Andrea Mostacci
- Zenghai Li, Sami Tantawi, Nathan Majernik
- Bruno Spataro
- Chad Pennington, Jared Maxxson